ISSN: 2639-7536

Research Article

Petroleum and Chemical Industry International

A Metallurgical Understanding of Welding Electrode Specifications for High Strength Steels

K Sampath*

Independent Consultant at Creative Concepts Proper selection of welding process, USA

***Corresponding Author**
K Sampath, Independent Consultant at Creative Concepts Proper selection of welding process, USA.

Submitted: 2025, Dec 29; **Accepted:** 2026, Jan 21; **Published:** 2026, Feb 06

Citation: Sampath, K. (2026). A Metallurgical Understanding of Welding Electrode Specifications for High Strength Steels. *Petro Chem Indus Intern, 9*(1), 01-26.

Abstract

High-strength steel (HSS) welding electrode specifications offer two sets of Tables for compliance, one on Specified Electrode Chemical Composition Requirements and second on Specified Minimum Weld Mechanical Properties Requirements. These sets of Tables may appear mutually exclusive but underlying metallurgical principles keep them inter-dependent. Suppressing austenite transformation-start (T_S) temperature simultaneously increases both strength and low-temperature Charpy V-notch (CVN) impact (or fracture) toughness of HSS weld metal (WM).

Specifically, a two-step approach is useful in understanding the metallurgy of high-strength, high-performance electrodes and WMs. This approach includes calculated austenite transformation-start (T_S) temperatures such as A_{r3}, B_S or M_S, besides carbon content, Yurioka's carbon equivalent number (CEN) and balanced Ti, B, Al, N, O additions, that correlate identified WM chemical composition with desired high-performance microstructures to meet or exceed minimum WM tensile and CVN impact (or fracture) toughness property requirements.

The first step uses a set of constitutive (statistical/regression) equations to control the amounts of principal alloy elements such as C, Mn, Cr, Ni, Mo, and Cu so the relevant calculated austenite transformation-start (T_S) temperatures such as A_{r3}, B_S, or M_S and Yurioka's CEN stay in a desirable range relative to the base metals being joined. While doing so, one also needs to ascertain that the common progression of calculated austenite transformation-start (T_S) temperatures wherein $A_{r3} > B_S > M_S$ remains valid.

The second step requires balanced Ti, B, Al, N, O additions with a Ti/B ratio at 10:1, to further lower the actual austenite transformation-start (T_S) temperature compared to the calculated T_S temperature. Both a lower austenite transformation-start (T_S) temperature and a narrow start-to-finish (T_S–T_F) temperature range for austenite decomposition ensure exceptional CVN impact toughness. The balanced Ti, B, Al, N, O content can be ascertained using an artificial neural network (ANN) template offered by the Japan Welding Engineering Society (JWES) at its website. A Ti/B ratio at 10 seems to allow exceptional CVN impact (or fracture) toughness, and (Ti+B+Al+N+O) additions between 500 ppm (0.05 wt-%) and 600 ppm (0.06 wt-%) is consistent with a lowering of austenite transformation-start (T_S) temperature. The JWES-ANN template allows one to manipulate 16 elements of the WM compositions, each within a specified range and seek a lower predictive temperature (T_{28J} / °C) below -80 °C for achieving 28 J absorbed energy during CVN impact testing.

1. Introduction

American Welding Society (AWS) offers several electrode specifications such as AWS *A5.1 Specification for Carbon Steel Electrodes for Shielded Metal Arc Welding, A5.5 Specification for Low-Alloy Steel Electrodes for Shielded Metal Arc Welding, A5.28 Specification for Low-Alloy Steel Electrodes and Rods for Gas Shielded Arc Welding*, etc. These and other similar high- strength steel (HSS) welding electrode specifications often have two sets

of Tables for compliance, one on Specified Electrode Chemical Composition Requirements and second on Specified Minimum Weld Mechanical Property Requirements. These two sets of Tables for compliance may appear standalone or mutually exclusive but underlying metallurgical principles keep them inter-dependent. These principles underscore the interactive effects of alloy elements in HSS that correlate chemical composition, processing during and after fusion welding, microstructure development with resultant mechanical properties such as weld metal (WM) tensile strength and Charpy V-notch (CVN) impact or fracture toughness.

The Table on Specified Electrode Chemical Composition Requirements for HSS specifies a range of alloy additions, with a low and a high end for each or most alloy additions. However, based on the lessons learned regarding the effects of "rich" electrode compositions on the hydrogen-assisted cracking (HAC) of the hull of the first *Seawolf* submarine in June and July of 1991 and structures involving earthquake-prone seismic locations pipelines for cold climate applications in northern Canada and arctic Russia, etc. one must avoid the selection of "rich" compositions within the required electrode specification range that could provide unusually high strength WM at low energy input welding conditions. Similarly, one must avoid the selection of "lean" compositions within the required electrode specification range that could provide abnormally poor strength WM at high energy input welding conditions [1-4].

A "rich" composition refers to most principal alloy elements such as C, Mn, Ni, Cr, Mo, and Cu at or near the top of the welding electrode specification range, while a "lean" composition refers to most of the above principal elements at or near the bottom of the welding electrode specification range. In this context, Sree Harsha Lalam's Ph.D. dissertation research at Cambridge University that developed an artificial neural network (ANN) model to predict six properties of ferritic WM may appear relevant [5,6]. These six WM properties included yield strength (YS), ultimate tensile strength (UTS), percent reduction of area (%RA), percent elongation (%El) and the test temperature required to achieve 100 J (T_{100J}/°C) and 28 J (T_{28J}/°C) absorbed energy during CVN impact testing. Lalam used two sets of databases in developing his ANN model: 1) a shielded metal arc (SMA) WM database on Fe-C-Mn steels produced under the direction of Dr. Glyn M. Evans, formerly with Oerlikon Welding Limited, Zurich, Switzerland augmented Evans's database with a vast and fairly general database assembled from publications on WM properties involving SMAW, submerged arc welding (SAW) and gas tungsten arc welding (GTAW) processes [7,8].

The Evans's SMA WM database was obtained from a single source that was collated from a monograph on the metallurgy of basic SMA WM deposits and uploaded to ResearchGate website in May 2017 This Fe-C-Mn database contains details of over 900 experimental SMAW electrodes and corresponding test results on WM chemical composition, all-weld-metal tensile properties and test temperature for CVN impact testing that achieved 28 J (i.e., T_{28J}/°C) and/or 100 J (i.e., T_{100J}/°C) absorbed energy [7,8].

The various individual SMAW electrodes cited in Evans's database mostly belonged to the "basic" type. The test weld deposits were produced by a single master welder, using standardized procedures, at Oerlikon Welding Limited, Zurich, Switzerland according to *ISO 2560- Welding Consumables — Covered Electrodes for Manual Metal Arc Welding of Non-Alloy and Fine Grain Steels — Classification*, at a heat-input of 1 kJ/mm, 200 °C interpass temperature and 20 mm plate thickness.

Figure 1 shows a typical macrograph of a standardized test weld belonging to the Evans's database, the CVN being centrally located as shown by the vertical red line, as specified in relevant standards [9].

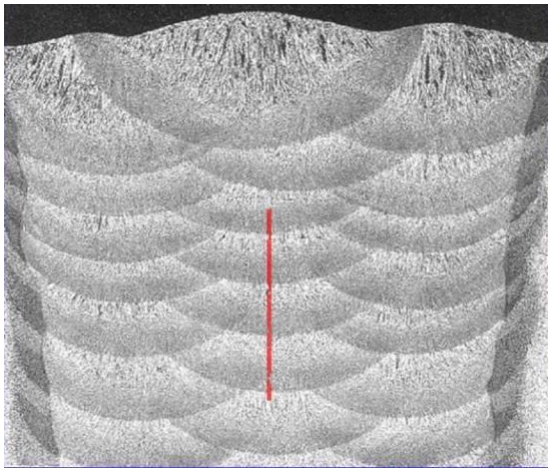

Figure 1: Cross-section of a standardized test weldment with three beads per layer [9].

Lalam's ANN model based on Fe-C-Mn WM database used sixteen alloy element additions in iron. Figure 2 shows one of the interactive models on T_{100J} /°C and T_{28J} /°C CVN absorbed energy involving both Mn and Ni contents. This contour plot predicted a hot spot at about 4 wt-% Ni when the Mn content was reduced to 0.5 wt-%. However, in the complete absence of Ni, extremely poor notch toughness was predicted at 1.6 wt-% Mn, i.e., corresponding to AWS E7018, thereby reinforcing the need to avoid the selection of "rich" and "lean" electrode compositions.

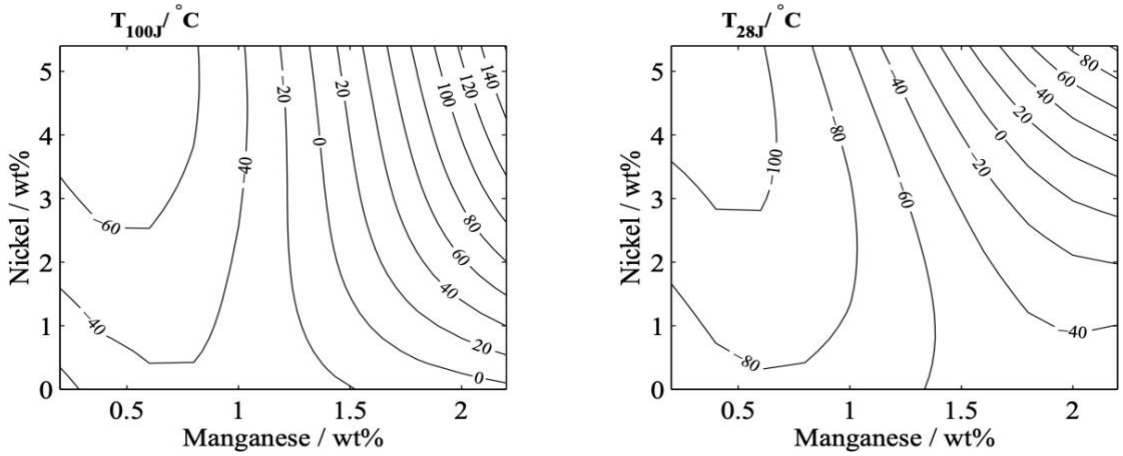

Figure 2: Generated CVN test temperature models: a) T_{100J} / °C; b) T_{28J} /°C.

Input Element	Minimum	Maximum
Carbon (wt-%)	0.035	0.152
Manganese (wt-%)	0.23	2.10
Silicon (wt-%)	0.01	1.11
Sulfur (wt-%)	0.003	0.046
Phosphorus (wt-%)	0.003	0.040
Nickel (wt-%)	0.03	5.48
Chromium (wt-%)	0.03	3.5
Molybdenum (wt-%)	0.005	1.16
Copper(wt-%)	0.02	2.04
Columbium i.e., Niobium (ppm)	3.0	980
Vanadium (ppm)	3.0	2873
Titanium (ppm)	2.0	1000
Boron (ppm)	1.0	200
Aluminum (ppm)	1.0	680
Nitrogen (ppm)	35.0	270
Oxygen (ppm)	217.0	1180
All Weld Metal Mechanical Properties		
Yield Strength (MPa, or N/mm^2)	350	1026
Ultimate Tensile Strength (MPa, or N/mm^2)	404	1123
Elongation (%)	10.5	35.8
Reduction in Area (%)	21	87.8
Temperature (T_{100J}) at 100 J (°C)	-89	45
Temperature (T_{28J}) at 28 J (°C)	-114	53

Table 1: Ranges of Fe-C-Mn Weld Metal Chemical Analysis and All-Weld Metal Mechanical Properties

Table 1 lists the individual ranges of the sixteen alloy element additions along with the ranges for the above six WM properties [5-9]. In particular, the Mn content ranged between 0.23 wt-% and 2.10 wt-% while the Ni content ranged between 0.03 wt-% and 5.48 wt-%. Lalam's ANN modeling included several predictive interactive models. Secondly, in January 1994, the Northridge, California earthquake caused unexpected damage to several welded steel-framed buildings in the greater Los Angeles area. Detailed examination of various weld fractures revealed that welding consumables, particularly self- shielded flux cored arc welding (FCAW-S) consumables, overall structural design, connection design, connection details, materials including both base metal (BM) and WM, workmanship and inspection must be controlled to ensure a system that remains reliably resistant to seismic forces in demand critical applications.

The above instances reveal a dire need to consolidate existing metallurgical knowledge on chemical composition of welding electrodes-fusion weld processing-microstructure development and mechanical properties of HSS and associated WMs. Fusion welding is a complex, secondary method of fabrication, as it involves a variety of controllable essential variables as outlined in the current edition of ASME Boiler Pressure Vessel Code - Section IX for various fusion welding processes. Here, as in Evans's SMA WM database, mechanical property test results generated using a standardized welding procedure involving joint geometry, energy input, bead sequence, etc. are extremely desirable to establish baselines and to allow ready comparisons. Given the type and value ranges of essential variables associated with any fusion welding process, one might wonder how could anyone avoid the selection of "rich" and "lean" compositions, yet meet or exceed WM tensile strength and CVN impact toughness requirements of a welding electrode specification?

2. Objectives

The objectives of the current effort are to:

1) Recommend a judicious use of major and minor alloy additions to welding electrodes that suppress austenite transformation-start (T_S) temperature and simultaneously increase both strength and low-temperature impact or fracture toughness of HSS WM; and

2) Offer specific means to achieve the above objectives using a two-step approach while complying with specified electrode chemical composition requirements.

Austenite transformation-start (T_S) temperature refers to nucleation and growth of product phases such as ferrite, pearlite, bainite, martensite, etc. from the parent austenite phase on cooling, while austenite transformation-finish (T_F) temperature refers to complete transformation of austenite, meaning zero or near-zero residual austenite content.

Incidentally, to date, the phrase "austenite transformation-start (T_S) temperature" and the need for suppressing or lowering the various austenite transformation-start (T_S) temperatures are not directly mentioned in HSS welding electrode specifications.

3. Transformation-Start Temperature

An understanding of the interactive effects of alloy elements in HSS WMs is necessary to enable one to navigate welding electrode specifications. Suppressing austenite decomposition or transformation to lower temperatures is known to induce greater nucleation rates and refine resultant microstructural constituents [10]. How does one suppress various austenite decomposition temperatures?

In general, there are two means available, first through proper control of chemical composition (of electrode and WM), and second by increasing (weld) cooling rate, depending on weld process selection, to obtain significant undercooling.

Figure 3 illustrates the relationship between 3 types of austenite transformation temperatures and UTS of regularly processed steels with 3 types viz., ferritic-pearlitic, bainitic and martensitic of predominant microstructures [11,12]. An approximate interpolation of the data obtained from Fig. 3 shows the UTS of ferritic-pearlitic steels appeared to range between 400 MPa and 550 MPa while the corresponding transformation temperature appeared to range between 900 °C and 670 °C. The UTS of bainitic steels appeared to range between 500 MPa and 1150 MPa while the corresponding transformation temperature appeared to range between 670 °C and 430 °C. In comparison, the UTS of martensitic steels appeared to exceed 1150 MPa while the corresponding transformation temperature appeared to be lower than 430 °C.

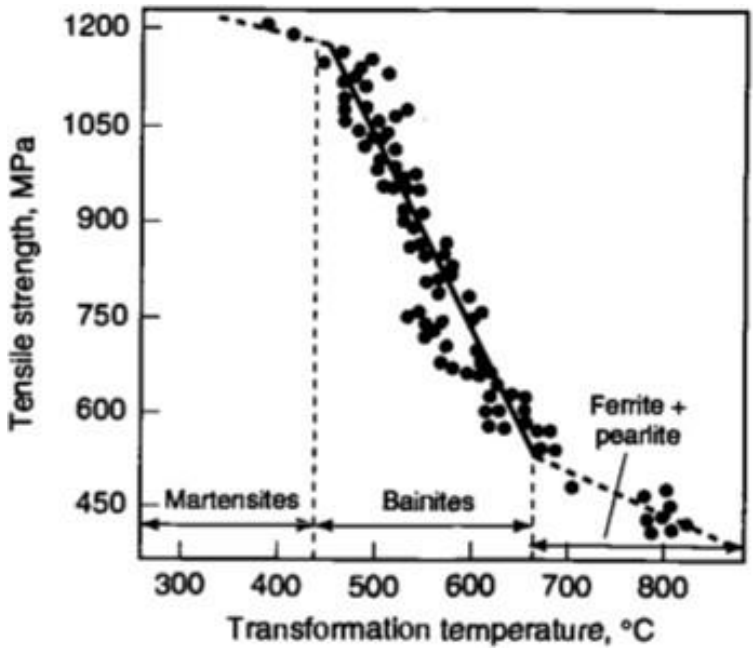

Figure 3: Relationship between ultimate tensile strength (in MPa) and transformation temperature (in °C) of ferrite-pearlite, bainitic and martensitic steels [11,12].

Interestingly, these ranges allow one to limit data selection when performing regression analysis of a suitable database, or augmented databases, including US Patent 6565678, "Weld metals with superior low temperature toughness for joining high strength, low alloy steels," https://patentimages.storage.googleapis.com/4f/70/c7/1b209b7c7e7f4a/US6565678.pdf.

The interactive effects of both principal and micro-alloy elements are known to affect relevant austenite decomposition-start (T_S) temperatures besides affecting Yurioka's Carbon Equivalent Number (CEN) as proposed by Yurioka, Suzuki, Ohshita and Saito [13]. It is well known that the austenite transformation-start (T_S) temperatures are a function of alloy additions, prior austenite grain size, cooling rate and possibly prior thermomechanical processing history. Control of both austenite decomposition temperatures and Yurioka's CEN is essential to simultaneously improve WM strength and CVN impact or fracture toughness. Lowering the austenite decomposition temperatures is known to refine matrix grain size and various microstructural constituents, thus simultaneously improving both strength and toughness while keeping carbon content much below 0.12 wt-% and reducing Yurioka's CEN are known to improve weldability of HSS.

The following constitutive (statistical/regression) equations relate various austenite decomposition temperatures such as Ouchi's A_{r3}, i.e., austenite-to-ferrite B_S, i.e., Bainite- start, B_{50}, i.e., 50% Bainite, B_F, i.e., Bainite-finish and M_S, i.e., Martensite-start with the contents of principal alloy elements [14,15].

A_{r3} (°C) = 910 – (310 x C) – (80 x Mn) – (80 x Mo) – (55 x Ni) – (20 x Cu) – (15 x Cr) (Eq. 1)

B_S (°C) = 830 – (270 × C) – (90 × Mn) – (37 × Ni) – (70 × Cr) – (83 × Mo) (Eq. 2)

B_{50} (°C) = 770 – (270 × C) – (90 × Mn) – (37 × Ni) – (70 × Cr) – (83 × Mo) (Eq. 3)

B_F (°C) = 710 – (270 × C) – (90 × Mn) – (37 × Ni) – (70 × Cr) – (83 × Mo) (Eq. 4)

M_S (°C) = 561 – (474 × C) – (33 × Mn)– (17 × Ni) – (17 × Cr) – (21 × Mo) (Eq. 5)

As shown above, Ouchi's A_{r3} temperature refers to Cu addition but other equations (2-5) including B_S, B_{50}, B_F, and M_S do not include Cu addition. The calculated B_S and B_F temperatures differ by 120 °C, and B_{50} temperature is midway between the calculated B_S and B_F temperatures. Equations 1 through 5 indicate that all principal alloy elements decrease austenite decomposition temperatures with carbon showing the highest coefficient. Keeping carbon content much below 0.12 wt-% is known to improve against HAC [16,17].

The above equations 1-5 were developed several decades ago and can be used to calculate or approximately estimate the transformation temperatures when cooling rate or critical cooling rate supposedly remains constant. However, these constitutive equations for austenite transformation-start (T_S) temperatures make no reference to prior austenite grain size, cooling rate, prior thermomechanical processing history and other micro-alloy additions such as Ti, B, Al, O, and N. For example, modern high-strength plate steels such as HSLA-65 (ASTM A945, Standard Specification for High-Strength Low-Alloy Structural Steel Plate with Low Carbon and Restricted Sulfur for Improved Weldability, Formability, and Toughness,) contain various micro-alloy additions such as Nb (Cb), V and Ti, under limited quantities.

Therefore, application of the above constitutive equations to obtain various calculated metallurgical characteristics (CMCs) such as austenite decomposition temperatures of modern steels offers only approximations of actual values. While the actual austenite TS and T_F temperatures (except M_F) can be measured using experimental techniques such as dilatometry, a new equation for austenite transformation-start or decomposition (T_S) temperature that likely includes the interactive effects of both principal and micro-alloy elements (in wt-%) and weld cooling rate (in °C/s) is extremely desirable.

To this end, a recent research effort employed Machine Learning algorithm to perform regression analysis of Evans's SMA WM database augmented with several other related datasets and identified the following a regression equation for *New* A_{r3} i.e., austenite-to- ferrite (T_S) temperature that includes all 14 elements, except P and S, in Evans's database:

New A_{r3} (°C)=906.49-2.78(CR)-439.3(C)+34.17(Si)-36.7(Mn)-8.5(Cu)-51.2(Ni)-27.08(Cr)-63.48(Mo)-1765.95(Nb)-520.29(V)-2401.12(Ti)-1784.44(B)+21.89(Al)+5300.15(N)-420.96(O)+297.07(C^2)-16.4(Mn^2)+11668.54(Nb^2)+458.21(√Ti)-1142.45(√N)+298.91(√O) (Eq. 6)

where CR refers to cooling rate in °C/s and various alloy elements are in wt-%. Adjusted R^2 of this equation is 0.9087. The standard error of the residuals is 24.89. The intercept value of this *New* A_{r3} equation is close to 910 °C (as seen in Ouchi's equation). The 910 °C represents the A_{e3} (equilibrium austenite-ferrite transformation) temperature for pure iron [18].

The above equation for *New* A_{r3} included the interactive effects of 14 (except P and S) major and minor alloy elements (in wt-%) identified in Evans's SMA WM database besides weld cooling rate (in °C/s). The above equation for *New* A_{r3} included the interactive effects of 14 (except P and S) major and minor alloy elements (in wt-%), as identified in Evans's SMA WM database in addition to weld cooling rate (in °C/s).

The *New* A_{r3} equation (Eq. 6) shows that while addition of N in excess of 100 ppm (0.01 wt-%) is expected to increase the *New* A_{r3} temperature, additions of C, Nb, V, Ti and B can substantially lower the calculated values of *New* A_{r3} temperature, depending on weld process selection and associated weld CR, requiring proper control over the above six elemental additions. In particular, the above Eq. 6 for *New* A_{r3} temperature is relevant for the transformation of austenite to high-performance acicular ferrite (AF) microstructures in WM.

The above regression equation for *New* A_{r3} can meet certain numerical ranges or specific boundary conditions for CMCs such as Yurioka's CEN related to chemical composition and specific microstructural characteristics of interest. The constraints and their numerical ranges themselves underscore the metallurgical criteria that depending on the desired combination of WM microstructure such as acicular ferrite, low-C bainite, or lath martensite, welding electrode designers need to lower the relevant solid-state austenite-start (T_S) temperatures to improve WM strength and fracture toughness while simultaneously reducing carbon content but overmatching Yurioka's CEN with that of base metal(s) being joined to ensure improved weldability at required level of overmatching the tensile strength of the weldment [13].

The CMCs are related to the chemical composition of HSS thru various statistical (regression) equations. Welding electrode design engineers could identify and simultaneously solve the above set of regression equations in a "mutually inclusive" fashion to meet certain numerical ranges or specific boundary conditions for CMCs such as Yurioka's CEN *New* A_{r3}, B_S, B_F, M_S, etc. related to chemical composition and specific microstructural characteristics of interest. The constraints and their numerical ranges themselves underscore the metallurgical principle that depending on the desired WM microstructure, one needs to lower relevant solid-state austenite-start (T_S) decomposition temperatures to improve WM strength and CVN impact or fracture toughness while simultaneously reducing carbon content and overmatch Yurioka's CEN of the relevant BM to improve weldability and ensure overmatching of relevant BM UTS. The *New* T_S temperature ranges can be used as an effective tool for metallurgically designing or evaluating high-strength welding electrodes and achieving the desired microstructure of the resultant high-performance WM [13].

Besides one's ability to control both principal alloy elements and micro-alloy elements, welding electrode designers can be concerned with the type and amount of other alloy elements such as S, P, Si, Nb (Cb), V, Zr, etc. The control of these other elements and the total gas (hydrogen, nitrogen and oxygen) content is critical to ensure better weldability, i.e., eliminate weld defects and promote desirable combinations in WM microstructure development. Depending on their nominal content and actual effects during welding, these other elements could further non-discriminately suppress the actual austenite-start (T_S) temperatures, thereby promote a "cloudburst" of solid-state phase transformation over a narrow (T_S-T_F) temperature range, particularly when the N content is held below 100 ppm (0.001 wt-%) [19,20] .

4. Carbon Equivalent

The welding literature offers several constitutive equations to calculate Carbon Equivalent and estimate the weldability of various types of high-strength steels, primarily to evaluate their sensitivity to HAC and to select conditions and parameters for enforcing appropriate low-hydrogen fusion welding practices. In this regard, the three widely used constitutive equations are:

P_{cm} = C + Si/30 +(Mn + Cu + Cr)/20 + Ni/60 + Mo/15 + V/10 + (5 x B) (Eq. 7)

developed by Ito and Bessyo (Ref. 20), primarily for pipeline steels.

CE_{IIW} = C + (Mn + Si)/6 + (Cr + Mo + V)/5 + (Ni + Cu)/15 (Eq. 8)

Is used for a variety of structural steels. The CE_{IIW} equation is a simplified form of Dearden and O'Neill's original formula for

hardenability that was subsequently adopted by the International Institute for Welding (IIW) in 1967 and became a generally accepted measure of steel weldability [21].

The CEN developed by Yurioka, Suzuki, Ohshita, and Saito is used for various types of structural steels, pipeline steels, pressure vessel steels, etc.:

$$CEN = C + \{A(C) \times EMU\} \quad \text{(Eq. 9)}$$

where A(C) refers to the Accommodation factor that is a function of C content, while EMU refers to a set of elemental multiplication unit involving Si, Mn, Cu, Ni, Cr, Mo, V, Nb (Cb) and B.

$$A(C) = 0.75 + 0.25 \tanh [20 \times (C - 0.12)] \quad \text{(Eq. 10)}$$

and

$$EMU = \{Si/24 + Mn/6 + Cu/15 + Ni/20 + (Cr + Mo + V + Nb)/5 + 5 \times B\} \quad \text{(Eq. 11)}$$

The above Yurioka's CEN constitutive equations include V, Nb (Cb) and B micro-alloy additions, besides various principal alloy elements, viz., C, Mn, Cr, Ni, Mo, and Cu. Equations 9 through 11 indicate that 10 alloy additions increase the Carbon Equivalent Number of HSS.

Based on the welding electrode classification requirements for WM strength and toughness, the desired WM microstructure could be either predominantly diffusional transformation products (such as acicular ferrite) when the desired WM strength is 700 MPa (100 ksi) or below, or predominantly athermal transformation products (such as bainite and/or martensite) when the desired WM strength is much higher than 700 MPa (100 ksi). In this continuum, one must realize that indiscriminate lowering of various austenite-start (T_S) temperatures could result in violation of the common progression of transformation temperatures, wherein $A_{r3} > B_S > B_F > M_S$, and lead to adverse consequences, particularly on as-welded WM toughness when diffusional transformation products are desired in WM microstructure. When athermal transformation products are desired in WM microstructure, one could consider suitably manipulating the differences among the calculated values of ($B_S - M_S$), ($B_{50} - M_S$), or ($B_F - M_S$) temperatures, with calculated difference in ($B_F - M_S$) temperatures lower than -50 °C [22].

In this context, Oak Ridge National Laboratories (ORNL), along with US Army Combat Capabilities Development Command Ground Vehicle Systems Center reported on their evaluation of a new set of Low-Temperature Phase Transformation (LTPT) welding consumables with three different welding processes—GMAW, GTAW and hot wire GTAW, and found that martensitic WMs containing oxide inclusions exhibited relatively poor toughness at tensile strengths over 1100 MPa [23].

Besides one's ability to control both principal alloy elements and micro-alloy elements, welding electrode designers are also concerned with the type and amount of other alloy elements such as S, P, Si, Nb (Cb), V, Zr, etc. The control of these other elements and the total gas (hydrogen, nitrogen, and oxygen) content is critical to ensure better weldability, i.e., eliminate weld defects and promote desirable combinations in WM microstructure development. Depending on their nominal content, and in particular (Ti+B+Al+N+O) content and actual effects during welding, these other elements could further non-discriminately suppress the actual austenite-start (T_S) temperatures, thereby promoting a "cloudburst" of solid-state phase transformation over a narrow (T_S-T_F) temperature range.

5. Interactive Effects of Alloy Additions

Several controlled research studies had evaluated the interactive effects of specific alloying elements including manganese additions etc. over a broader range and identified the effects of minimum and maximum levels of the element(s) on microstructure development and in meeting or exceeding specific WM mechanical property requirements of HSS WMs. Such studies had varied primarily one or more alloy element(s) at a time but didn't evaluate the combined interactive effects of all alloy additions. Nevertheless, these studies often provide insightful metallurgical knowledge in understanding possible underlying mechanisms that facilitate the development of certain WM microstructures [24-30].

However, in multi-component Fe-C-Mn systems, the interactive effects of various alloy elements could likely undermine the "effective" operation of one or more such mechanisms and might not allow one to achieve the anticipated benefits in meeting or exceeding WM mechanical property requirements. For example, when thermodynamically feasible and kinetically favorable, Nb (Cb), Ti, V, Mo, W, Cr and Mn alloy additions form carbides in decreasing order, and thereby reduce carbon in solution, thus significantly decreasing the adverse effect of carbon on sensitivity to HAC.

Similarly, in multi-component Fe-C-Mn systems containing B, Mo, Ti and N, formation of BN (boron nitride) and $FeMo_2B_2$ boride could tie up B from solid-solution, thereby decreasing the hardenability effect of B [31]. One could also effectively prevent the formation of BN by alloying with Ti that preferentially binds N through the formation of titanium carbonitride Ti(C,N).

6. Computer Modeling of Weld Metals

In recent years, there have been a growing interest to develop computer models on WM mechanical properties, with a particular intent to predict WM tensile and impact or fracture toughness properties based on WM chemical composition and underlying physical metallurgy principles involving chemical composition, weld processing conditions, microstructure development and weld mechanical properties [32-45]. Such computer modeling efforts primarily involved ANNs which are emerging as very powerful tools with added capacity to reconstruct a database on weld properties through data selection and augmentation. Apparently, none of the above regression and ANN models attempted to correlate WM tensile and CVN impact toughness with WM chemical composition through austenite transformation-start (T_S) temperatures.

The Japan Welding Engineering Society (JWES) offers a website wherein one could calculate and predict the T_{28J} /°C for CVN impact toughness at 28 J absorbed energy of Fe-C-Mn SMA WMs based on their chemical composition, with certain minimum and maximum limits for specific elements [46]. The prediction uses an ANN software developed by D. J. C. MacKay at the University of Cambridge that is based on Evans's SMA WM database. The prediction is possible within the minimum and maximum limits for specific elements, as revealed in the JWES ANN template. The individual range for each of the 16 elemental additions are shown in Fig. 4. The ANN prediction gives maximum, minimum and average values of T_{28J} /°C along with the degree of prediction error. When the difference between the maximum and minimum predicted values is over 30 °C, the prediction is considered unreliable.

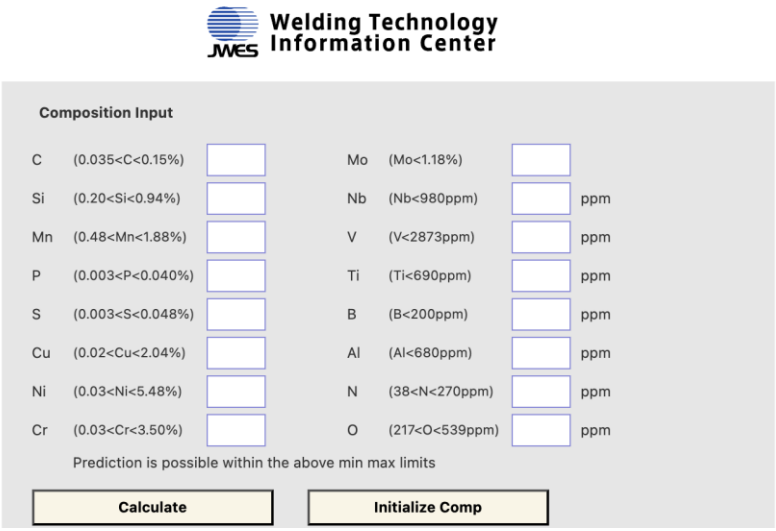

Figure 4: JWES-ANN Template with range for each elemental addition.

A key advantage of the JWES-ANN template is that it allows one to manipulate the values of 16 elements - (C, Si, Mn, P, S, Cu, Ni, Cr and Mo in wt-%, and Nb (Cb), V, Ti, B, Al, N, and O in ppm) - within certain minimum and maximum limits for each alloy element as in JWES- ANN template. The actual WM chemical composition would allow welding electrode designers to calculate and/or predict the T_{28J} /°C CVN test temperature of Fe–C–Mn-Ni WMs to achieve below -80 °C temperature.

Welding electrode design engineers could use the JWES-ANN template to manipulate the addition of 16 elements - C, Si, Mn, P, S, Cu, Ni, Cr and Mo in wt-%, and Nb (Cb), V, Ti, B, Al, N and O in ppm, each within a restricted range, to achieve high-performance microstructures with exceptional strength and CVN impact (or fracture) toughness. Despite the above clear advantage of the JWES-ANN template in substantially reducing the risk in achieving a colder T_{28J} /°C CVN test temperature, it is well-known that using a singular value of temperature for assessing the toughness behavior of HSS weldment might potentially lead to severe limitations. While the JWES-ANN tool allows one to substantially eliminate risk, the above limitation requires experimental verification to assess WM impact toughness behavior over a range of test temperatures, and to identify appropriate ductile-to-brittle transition temperature (DBTT).

Currently available correlation or relationship between WM UTS and WM chemical composition based on the *New* A_{r3} [i.e., austenite-start (T_S) temperature] equation and weld cooling rate is expected to further complement the JWES-ANN template for predicting T_{28J} /°C for CVN absorbed energy based on WM chemical composition, thereby providing a pair of effective tools for efficient development of welding electrodes based on Fe-C-Mn system for high- performance or demand-critical applications.

Element	*New* A_{r3} Equation (Ref. 18)		JWES ANN Template (Ref. 46)	
	Minimum (wt-%)	Maximum (wt-%)	Minimum (wt-%)	Maximum (wt-%)
C	0.024	0.792	0.035	0.15
Si	0	2.04	0.2	0.94
Mn	0	2.52	0.48	1.88
P	0	0.11	0.003	0.040
S	0	0.046	0.003	0.048
Cu	0	2.04	0.02	2.04
Ni	0	3.49	0.03	5.48
Cr	0	2.8	0.03	3.50
Mo	0	1.11	0	1.18
Nb	0	0.098	0	0.098
V	0	0.099	0	0.2873
Ti	0	0.069	0	0.0690
B	0	0.02	0	0.020
Al	0	1.55	0	0.0680
N	0	0.0270	0.0038	0.0270
O	0	0.118	0.0217	0.0539
Cooling Rate (°C/s)	0.001	30	13	

Table 2: Minimum and Maximum Limits for Elemental Composition and Cooling Rate

Table 2 shows a numerical comparison of the minimum and maximum limits for elemental composition and cooling rate for the New Ar3 equation and the JWES-ANN template.

7. Metallurgical Design of Welding Electrodes

The early 1990s witnessed the successful development of a set of advanced ER-100S and ER-120S (MIL-100S and MIL-120S equivalents) high-performance solid wire electrodes for Gas Metal Arc (GMA) welding of HSS such as HY-100, HY-80, HSLA-100, HSLA-80 etc. used in U.S. Navy aircraft carrier and submarine construction [47-50]. This successful effort used an innovative approach that employed 3 specific aspects. First, it consolidated existing metallurgical knowledge on chemical composition-processing-microstructure development and mechanical properties of high-strength steels. Second, it reached beyond existing knowledge on electrode development and particularly avoided the selection of "rich" and "lean" compositions within the required chemical composition range of the electrode specification, AWS *A5.28 Specification for Low-Alloy Steel Electrodes and Rods for Gas Shielded Arc Welding*. Third, it involved the development and use of a constraints-based model, or CBM. The constraints refer to selection of numerical ranges for Yurioka's CEN, and A_{r3}, B_s, B_f, M_s temperatures, etc.

Electrode ID	C	Mn	Si	P	S	Cu	Ni	Cr	Mo	V	Ti	B	N	O	H (mL/100 g)
1	0.027	1.51	0.34	0.001	0.0019	0.001	2.52	0.02	0.52	0.001	0.033	0.001	0.0006	0.0069	2.11
2	0.028	1.49	0.37	0.002	0.0018	0.001	2.38	0.01	0.99	0.001	0.031	0.001	0.0009	0.0047	1.51
3	0.028	1.54	0.34	0.001	0.0018	0.001	3.78	0.01	0.52	0.001	0.028	0.001	0.0010	0.0052	2.13
4	0.029	1.50	0.35	0.001	0.0018	0.001	3.73	0.01	0.98	0.002	0.030	0.001	0.0006	0.0078	1.46
5	0.030	1.82	0.34	0.001	0.0020	0.001	2.37	0.01	0.52	0.003	0.029	0.001	0.0006	0.0076	1.63
6	0.029	1.82	0.35	0.002	0.0021	0.001	2.38	0.01	0.98	0.003	0.029	0.001	0.0007	0.0066	1.15
7	0.026	1.82	0.35	0.002	0.0022	0.001	3.77	0.01	0.51	0.002	0.027	0.001	0.0006	0.0064	1.79
8	0.030	1.80	0.33	0.002	0.0019	0.001	3.72	0.01	0.99	0.003	0.025	0.0003	0.0004	0.0082	1.23
High	0.030	1.82	0.37	0.002	0.0022	0.001	3.78	0.02	0.99	0.003	0.033	0.001	0.001	0.0082	2.13
Low	0.026	1.49	0.33	0.001	0.0018	0.001	2.37	0.01	0.51	0.001	0.025	0.0003	0.0004	0.0047	1.15
Range	0.004	0.33	0.04	0.001	0.0004	0	1.41	0.01	0.48	0.002	0.008	0.0007	0.0006	0.0035	0.98

Table 3: Chemical composition (in wt-%) of 8 experimental solid wire GMAW electrodes based on 2^3 Taguchi design

Table 3 shows the chemical composition (in wt-%) of 8 experimental solid wire GMAW electrodes that were based on 2^3 Taguchi design. The 2^3 Taguchi design varied the contents of only three principal alloy elements, viz., Manganese, Nickel, and Molybdenum, each at 2 levels, one "high" and the other "low," while keeping all other elements at a fairly constant level. Vacuum Induction Melting (VIM) was used to produce various billets corresponding to the 8 bare solid wire electrode manufacturing, all in one-go, thus eliminating conventional "trial-and-error" methods. Use of VIM limited the total gas content much below 500 ppm (0.05 wt-%) and eliminated any adverse effect of gaseous elements on WM toughness.

One of the solid wire electrodes (#3 with 0.028 wt-% C, 1.54 wt-% Mn, 3.78 wt-% Ni, 0.52 wt-% Mo, 0.34 wt-% Si, 0.01 wt-% Cr, 0.028 wt-% Ti, 0.0001 wt-% B, O_2 at 52 ppm, N_2 at 10 ppm, H_2 at 2.13 mL/100g and with the following CMCs: CEN = 0.32; B_{50} = 440 °C, M_S = 422 °C) was used in additional evaluations of a set of 8 GMA weldments.

Weld #	Base Plate	Energy Input (kJ/ in.)	Welding Position	Metal Transfer	Preheat Temp (°F)	Interpass Temp (°F)	Calculated Weld Cooling Rate (°F/s)	Weld YS (MPa)
1	HSLA-100	30	Flat	Spray	125	125	95	786
2	HSLA-100	45	Flat	Spray	150	150	57	751
3	HY-100	45	Flat	Spray	150	150	57	746
4	HSLA-100	55	Flat	Spray	125	125	47	729
5	HSLA-100	110	Flat	Spray	125	125	11	638
6	HSLA-100	110	Uphill	Pulsed	300	300	7	600
7	HSLA-100	110	Flat	Spray	300	300	5	609
8	HY-100	110	Flat	Spray	300	300	5	600

Table 4: Eight Experimental Welds Produced Using Solid Wire GMAW Electrode #3

As shown in Table 4, these weldments were produced in 25.4 mm (1-in.) thick HSLA-100 and HY-100 steel plates using a wide range of shipyard fabrication conditions that represented calculated weld cooling rates ranging between 3 °C/s and 53 °C/s at 538 °C (i.e., 1000 °F). As shown in Fig. 5, these 8 weldments revealed acceptable variation in WM yield strength with calculated weld cooling rate at 538 °C in line with U.S. Navy requirements. The trend line showed the following statistical relationship, at a r^2 value of 0.99:

$$\text{WM YS (in MPa)} = 542.6 \times (\text{Calculated weld cooling rate at 538 °C})^{0.0925} \quad \text{(Eq. 12)}$$

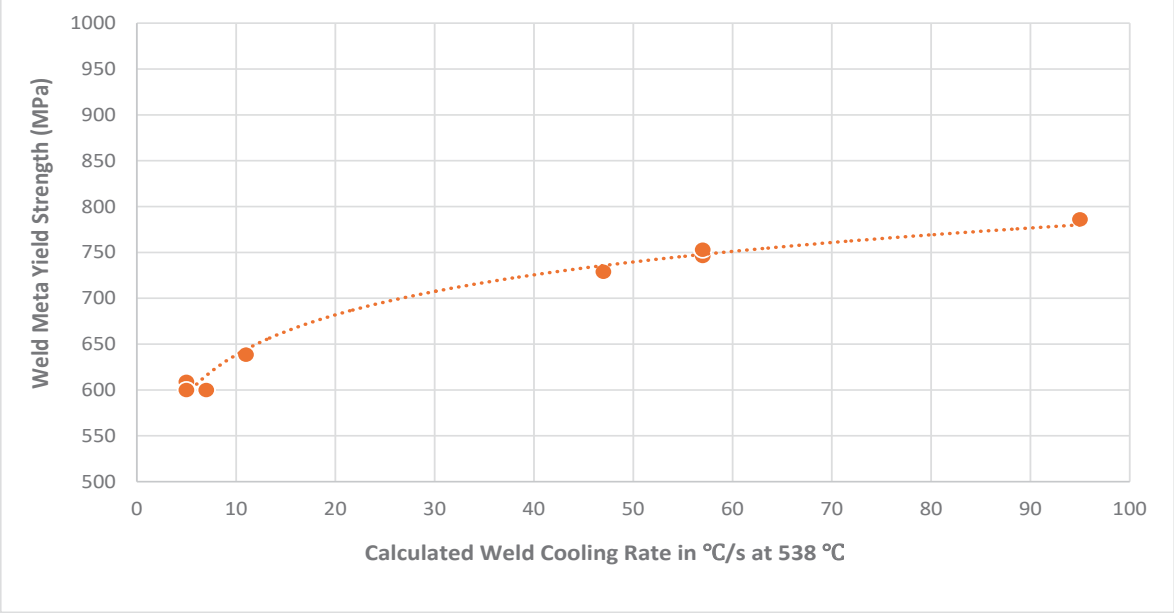

Figure 5: Variation of yield strength of HSS WM with calculated weld cooling rate.

As mentioned earlier, these CMCs are related to the chemical composition of HSS thru approximated statistical (regression) equations. CBM identifies and simultaneously solves the above set of regression equations in a "mutually inclusive" fashion to meet certain numerical ranges or specific boundary conditions for CMCs such as Yurioka's CEN, A_{r3} , B_s, B_F, M_S, etc. related to chemical composition and specific microstructural characteristics of interest, as shown in Fig. 3. The constraints and their numerical ranges themselves underscore the metallurgical principle that depending on the desired WM microstructure, one needs to lower relevant solid-state austenite decomposition (T_s) temperatures to improve WM strength and CVN impact or fracture toughness while simultaneously reducing carbon content and CEN to improve weldability.

Following the award of U.S. the related research on the actual chemical compositions of the 8 experimental electrodes was published The WMs showed a predominantly bainitic microstructure that was also insensitive to HAC. Thus, the use of CBM approach in successfully developing high performance solid electrodes for GMA welding of HY-100, HY-80, HSLA-100, HSLA-80 steels per relevant Military standards for BMs and welding electrodes substantially eliminated risk, reduced cost while meeting stringent schedule requirements [51-53].

The CBM approach clearly demonstrated that selected austenite-start (T_S) temperature ranges can be used as an effective tool for metallurgically designing high-strength welding electrodes and achieving the desired microstructure of the resultant high-performance WM while avoiding the selection of "rich" and "lean" electrode compositions as listed in the relevant MIL-E-23765/2E specifications. The various calculations associated with this metallurgical and mathematical modeling can be performed using either a scientific calculator, commercially available Microsoft Excel or similar software, or a suitably designed computer software program. Figure 6 shows a typical flowchart used to identify electrode or WM compositions with desired minimum and maximum range of limits as detailed in the boundary conditions for various elements within an electrode specification and the boundary conditions for desired CMCs of WM [54,55].

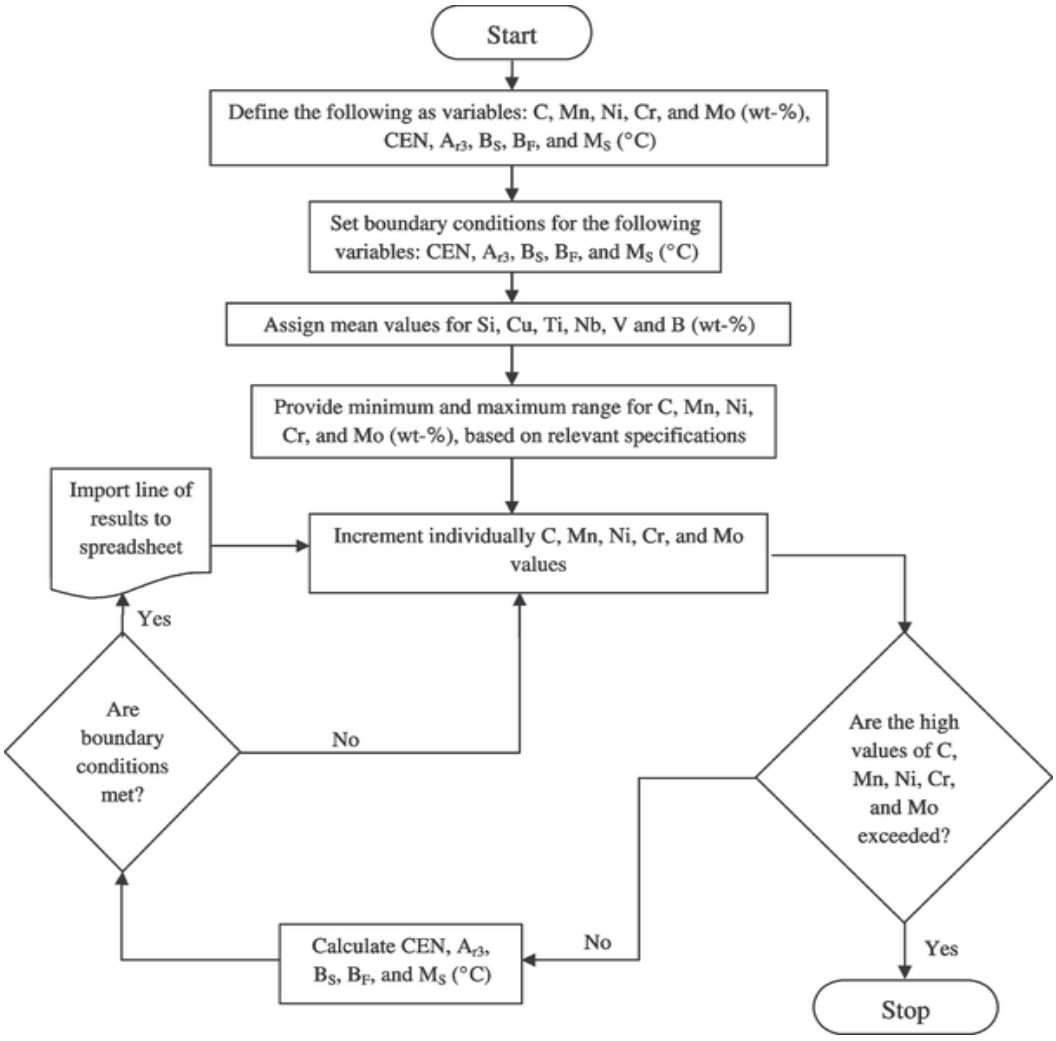

Figure 6: A typical flowchart used with computer programming associated with CBM.

8. Balancing Ti-B-Al-N-O Additions

A subsequent research publication on "Analysis of A High-Strength Steel SMAW Database," demonstrated that CBM could be applied to the efficient analysis of Evans's SMA WM database. This analysis allowed classification and/or ranking of all WMs in the Fe-C-Mn database using selected CMCs thereby reaffirmed that controlling carbon content, value of CEN, and relevant calculated austenite-start (T_S) temperatures, particularly the difference between the calculated B_S, B_F and M_S temperatures, was critical in developing and identifying high-performance, high- strength steel welding electrodes.

A part of Evans's Fe-C-Mn SMA WM database used a separate or an independent scheme to build a total of 24 SMA welds, with Ti-B-Al-N-O additions These 24 welds included a set of 8 welds, each corresponding to 3 levels of nitrogen content – normal (below 85 ppm or 0.0085 wt-%), intermediate (120 ppm to 164 ppm or 0.012 to 0.0164 wt-%), and high (217 ppm to 249 ppm or 0.0217 to 0.0249 wt-%). While C, Mn and Si contents varied over a narrow range, rest of the principal alloy elements were essentially held constant. The primary intent of this subset of WMs was to identify and correlate the effects of Ti-B-Al-N-O additions on WM tensile strength, CVN impact toughness and microstructure development in the fusion zone and reheated weld metal [56,57].

The first part of Evans's SMA WM database used an independent scheme to build a first set of 8 SMA WMs based on a TiBAlN series with N content below 85 ppm (0.0085 wt-%). These 8 WMs were named O, W, X, Y, Z, T, U, and V. Weld W is considered somewhat similar to WMs deposited using Oerlikon's Tenacito 38R SMA welding electrode, currently manufactured by Lincoln Electric Company. This subset of 8 WMs focused on identification and correlation of the effects of Ti-B-Al-N-O micro-alloy additions on WM tensile properties, CVN impact toughness, and microstructure development in the fusion zone with reheated WM, in multi-pass welding.

Heat ID	C	Si	Mn	P	S	Ti	B	Al	N	O	(Ti+B+Al+N+O) (wt-%)	Ti/B Ratio	Yurioka's CEN
O	0.074	0.25	1.4	0.007	0.008	0.0001	0.0001	0.0006	0.0079	0.0475	0.0562	1	0.219
O2	0.073	0.27	1.66	0.008	0.009	0.0005	0.0005	0.0005	0.0235	0.0399	0.0649	1	0.243
X	0.069	0.45	1.47	0.006	0.005	0.041	0.0002	0.0001	0.0077	0.0282	0.0772	205	0.223
X2	0.068	0.47	1.46	0.006	0.007	0.045	0.0002	0.0005	0.0249	0.0297	0.1003	225	0.221
Y	0.07	0.45	1.57	0.01	0.006	0.039	0.0039	0.0013	0.0083	0.0308	0.0833	10	0.244
Y2	0.069	0.36	1.51	0.008	0.007	0.041	0.0044	0.0005	0.0232	0.0292	0.0983	9.3	0.236
Z	0.072	0.49	1.56	0.01	0.007	0.042	0.0048	0.016	0.0067	0.0438	0.1133	8.75	0.250
Z2	0.068	0.5	1.45	0.011	0.006	0.047	0.0045	0.018	0.023	0.044	0.1365	10.44	0.232
U	0.073	0.4	1.52	0.011	0.006	0.039	0.0158	0.0005	0.0084	0.029	0.0927	2.47	0.277
U2	0.066	0.36	1.4	0.012	0.007	0.039	0.0167	0.0005	0.0217	0.0297	0.1076	2.34	0.255
V	0.078	0.6	1.44	0.007	0.006	0.054	0.0056	0.058	0.0041	0.044	0.1657	9.64	0.254
V1	0.067	0.63	1.44	0.01	0.005	0.048	0.0044	0.056	0.012	0.0473	0.1677	10.91	0.232
V2	0.069	0.6	1.42	0.012	0.006	0.043	0.0035	0.056	0.0235	0.0470	0.173	12.29	0.231

Six of other sixteen alloy additions were kept constant: Cu at 0.03 wt-%, Ni at 0.03 wt-%, Cr at 0.03 wt-%, Mo at 0.005 wt-%, Nb at 5 ppm (0.0005 wt-%) and V at 5 ppm (0.0005 wt-%).

Table 5: Chemical Composition (in wt-%) of Thirteen WMs

Table 5 shows the Ti-B-Al-N-O chemical composition of 13 SMA WMs belonging to TiBAlN series, with three levels of N content along with their total (Ti+B+Al+N+O) content in wt-%, Ti/B ratio and Yurioka's CEN. The carbon content of each of these 13 WMs ranged between 0.066 wt-% and 0.078 wt-%. The Si content of these 13 WMs varied between 0.25 wt-% and 0.63 wt-% and Mn content varied between 1.40 wt-% and 1.66 wt-%. Other principal alloy elements remained constant: Cu content at 0.03 wt-%, Ni content at 0.03 wt-%, Cr content at 0.03 wt-%, Mo content at 0.005 wt-%, Nb content at 5 ppm (0.0005 wt-%) and V content at 5 ppm (0.0005 wt-%). Yurioka's CEN of these 13 WMs ranged from a low of 0.219 for weld O to a high of 0.277 for weld U.

Of the 13 SMA WMs belonging to the TiBAlN series, Ti content varied between 1 ppm (0.0001 wt-%) and 540 ppm (0.0540 wt-%), B content ranged between 1 ppm (0.0001 wt-%) and 167 ppm (0.0167 wt-%), Al content varied between 1 ppm (0.0001 wt-%) and 580 ppm (0.0580 wt-%), N content varied between 41 ppm (0.0041 wt-%) and 249 ppm (0.0249 wt-%) and O content varied between 282 ppm (0.0282 wt-%) and 475 ppm (0.0475 wt-%). The combined (Ti+B+Al+N+O) content of these 13 WMs ranged from a low at 562 ppm (0.0562 wt-%) for weld O to a high at 1730 ppm (0.173 wt-%) for weld V2. As shown in Table 5, the Ti/B ratio of these 13 WMs ranged between 1 for weld 0 and O2, and 225 for weld X2. Coincidentally, weld Y showed a Ti:B ratio at 10:1.

8.1 Weld Mechanical Properties

Weld ID	Ti (wt-%)	B (wt-%)	Al (wt-%)	N (wt-%)	O (wt-%)	(Ti+B+Al+N+O) (wt-%)	Dilatometric Transformation Temperature (°C)				
							T_S	T_{50}	T_{PRTT}	T_F	(T_S- T_F)
O	0.0001	0.0001	0.0006	0.0079	0.0475	0.0562	762	658	650	554	208
O2	0.0005	0.0005	0.0005	0.0235	0.0399	0.0649	754	630	606	534	220
X	0.041	0.0002	0.0001	0.0077	0.0282	0.0772	760	660	630	568	192
X2	0.045	0.0002	0.0005	0.0249	0.0297	0.1003	760	650	638	572	188
Y	0.039	0.0039	0.0013	0.0083	0.0308	0.0833	710	625	618	560	150
Y2	0.041	0.0044	0.0005	0.0232	0.0292	0.0983	703	612	606	510	193
Z	0.042	0.0048	0.016	0.0067	0.0438	0.1133	710	645	642	550	160
Z2	0.047	0.0045	0.018	0.023	0.044	0.1365	703	635	632	560	143
U	0.039	0.0158	0.0005	0.0084	0.029	0.0927	700	626	620	531	169
U2	0.039	0.0167	0.0005	0.0217	0.0297	0.1076	765	662	650	574	191
V	0.054	0.0056	0.058	0.0041	0.044	0.1657	680	598	596	507	173
V1*	0.048	0.0044	0.056	0.012	0.0473	0.1677	760	680	640	555	205
V2	0.043	0.0035	0.056	0.0235	0.047	0.173	754	644	642	588	166
Low	0.0001	0.0001	0.0001	0.0041	0.0282	0.0562	680	598	596	507	143
High	0.054	0.0167	0.058	0.0249	0.0475	0.173	765	680	650	588	220
Range	0.0539	0.0166	0.0579	0.0208	0.0193	0.1168	85	82	54	81	77

* The transformation temperature for weld V1 obtained from interpolation of graphical data reported in Ref. 60.

Table 6: Selected Transformation Temperatures of Thirteen WMs with Ti-B-Al-N-O Additions

N. Ilman, et al. performed dilatometric evaluation of 13 of these 24 WMs [58-60]. These 13 WMs, as shown in Table 6, were selected to allow dilatometric evaluation of specific alloy additions relative to the above range of Ti, B, Al, N and O additions, particularly the effect of N content at 3 levels on both T_S and T_F temperatures.

The dilatometric evaluation studied the austenite-to-acicular ferrite (AF) transformation at both start and finish temperatures (T_S and T_F) during continuous cooling. Test specimens were machined to form hollow cylinders with the following dimensions: 10 mm long by 5 mm outside diameter with 1 mm wall thickness. The axis of the test specimen was maintained parallel to the original welding direction. The specimens were subjected to the following controlled thermal cycle: austenitization at 1250 °C for 2 minutes, followed by continuous cooling at a typical (weld) cooling rate of 13 °C/s from 800 °C to 500 °C (i.e., 8/5). The study determined T_S, 50% transformation (T_{50}), peak rate transformation (T_{PRTT}) and T_F temperatures of the 13 (O, O2, X, X2, Y, Y2, Z, Z2, U, U2, V, V1 and V2) WMs. Weld W is considered somewhat similar to WMs deposited using Oerlikon's Tenacito 38R[2] SMA welding electrode, currently manufactured by Lincoln Electric Company. The T_S and T_F temperatures at 13 °C/s weld cooling rate of weld W were determined using dilatometry at a typical weld cooling rate of 13 °C/s.

Apparently, welding electrode designers need to assess the toughness behavior of WMs with more than 100 ppm (0.001 wt-%) N and try to correlate "unbalanced" (Ti+B+Al+N+O) contents and specific aspects of WM microstructure [61]. Prior research on flux-cored arc WMs had attributed a significant decrease in low-temperature impact toughness to excessive Ti and B contents that resulted in an increased volume content of upper bainite [62].

A comparison of welds Y and Z revealed that at the same low, experimentally determined T_S (i.e., A_{r3}) temperature at 710 °C. Here, one could use Ti:B at 10:1 ratio, as in weld Y, and lesser amounts of (Ti+B+Al+N+O) content to achieve further lowering of both ($T_S - T_F$) temperature range and the T_{28J}/°C test temperature for achieving 28 Joules absorbed energy during CVN impact testing.

The dilatometric studies by were crucial in determining the Ti–B–Al–N–O addition at 833 ppm (0.0833 wt-%) in weld Y which appeared to provide a "near" balance that was effective in producing a narrower (T_S–T_F) temperature at 150 °C, further enabling a "cloudburst" of solid-state phase transformation of austenite to acicular ferrite (AF), resulting in refined microstructural features. Due to this metallurgical effect, weld Y achieved:

1) a low T_S temperature at 710 °C due to specific WM chemical composition
2) a narrow (T_S–T_F) temperature at 150 °C due to a "nearly" balanced Ti-B-Al-N-O content at 833 ppm (0.0833 wt-%)
3) C content at 0.070 wt-%, much below 0.10 wt-%
4) Yurioka's CEN (Ref. 13) at 0.244

5) actual T_{28J}/°C of -114 °C
6) actual T_{100J}/°C of -84 °C, besides
7) YS/UTS ratio at 0.92.
The YS/UTS ratio appeared marginally higher than 0.90, as one might require YS/UTS ratio lower than 0.90 for demand-critical applications.

A recent research publication on two-stage selective analysis of Evans's SMA WM database shows how one could apply a constraints-based model (CBM) in relating WM chemical composition with the formation of predominantly AF microstructure in WM. Depending on the value of T_S temperature, at about 690 °C ± 40 °C as a desirable target range, with a Ti:B ratio held near 10:1, the total "balanced" Ti-B-Al-N-O additions could be held between 0.05 wt-% and 0.06 wt-% in achieving a significant spread between YS and UTS of WM while ensuring the YS/UTS ratio is held between 0.84 and 0.92 to provide a superior combination of excellent ductility and low-temperature impact (fracture) toughness [63].

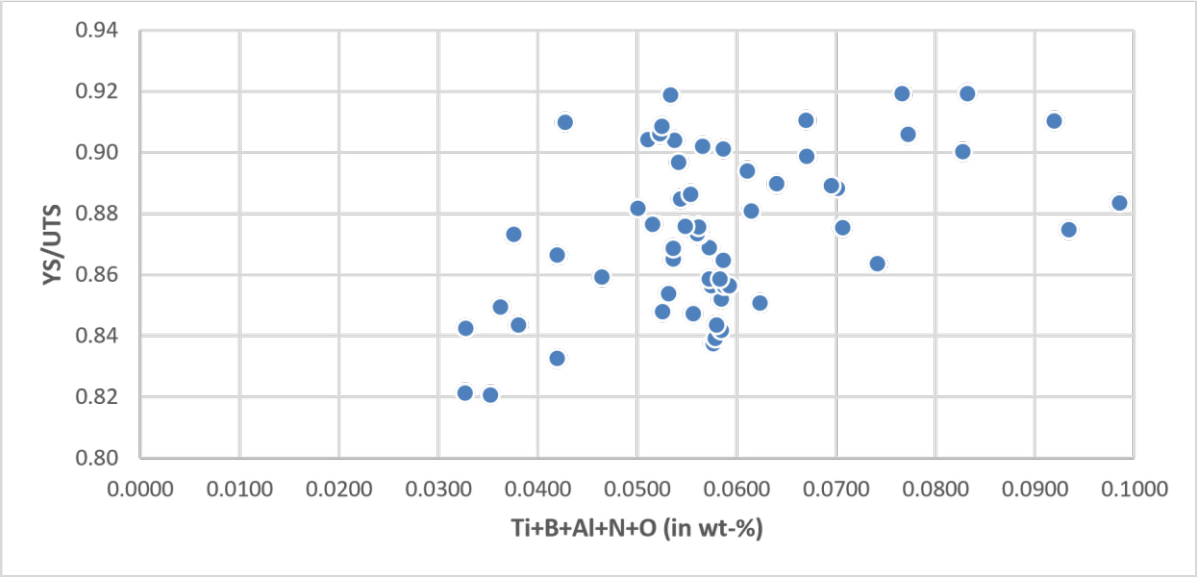

Figure 7: Clustered Results show Ti-B-Al-N-O Addition between 0.05 wt-% and 0.06 wt-% for Achieving YS/UTS ratio between 0.84 and 0.92 .

One could also lower the austenite-to-AF transformation (T_S) temperature by "balancing" Ti-B-Al-N-O microalloying additions with N content below 100 ppm (0.01 wt-%). The first-stage selective analysis considered 31 WMs in a multi-component Fe-C-Mn-based compositions that substantially improved UTS, showed a significant spread between YS and UTS, with YS/UTS ratio between 0.84 and 0.95 while significantly lowering the test temperature (T_{28J}/°C) for WM CVN impact toughness at 28 Joules between -114 °C and -100 °C. The second-stage selective analysis of Evans's SMA WM database involving a cluster analysis of Ti-B-Al-N-O content in 61 WMs (Fig. 7) revealed that the "balanced" (Ti+B+Al+N+O) microalloying additions could be held between 500 ppm (0.05 wt-%) and 600 ppm (0.06 wt-%) in achieving YS/UTS ratio between 0.84 and 0.92 while achieving a test temperature (T_{28J}/°C) for WM CVN impact toughness at 28 Joules between -114 °C and -90 °C.

The above selective analysis further asserted that as the actual or calculated T_S temperature is lowered, one could further lower the amounts of (Ti+B+Al+N+O) micro-alloying additions to achieve additional lowering of T_S temperature and test temperature (T_{28J}/°C) for WM CVN impact toughness at 28 Joules.

8.2 Mechanical Properties of Thirteen WMs with Ti-B-Al-N-O Additions

Weld ID	Selected Calculated Metallurgical Characteristics											
	P_{cm}	CE_{IIW}	CEN	A_{r3} (°C)	B_S (°C)	B_{50} (°C)	B_F (°C)	M_S (°C)	(B_F-M_S) (°C)	$(A_{r3}-B_S)$ (°C)	$(A_{r3}-B_{50})$ (°C)	$(A_{r3}-B_F)$ (°C)
O	0.157	0.360	0.219	772	680	620	560	479	82	92	152	212
O2	0.162	0.406	0.243	751	657	597	537	470	67	94	154	214
X	0.187	0.400	0.223	768	675	615	555	479	77	92	152	212
X2	0.194	0.401	0.221	769	677	617	557	479	77	92	152	212
Y	0.245	0.418	0.244	760	666	606	546	475	71	93	153	213
Y2	0.202	0.392	0.236	765	672	612	552	477	75	93	153	213
Z	0.186	0.425	0.250	760	667	607	547	474	72	93	153	213
Z2	0.171	0.404	0.232	770	678	618	558	480	78	92	152	212
U	0.162	0.404	0.277	763	670	610	550	475	75	93	153	213
U2	0.182	0.370	0.255	774	683	623	563	482	80	92	152	212
V	0.184	0.429	0.254	768	676	616	556	475	80	92	152	212
V1	0.235	0.423	0.232	771	679	619	559	481	78	92	152	212
V2	0.181	0.417	0.231	772	680	620	560	480	80	92	152	212
Low	0.157	0.36	0.219	751	657	597	537	470	67	92	152	212
High	0.245	0.429	0.277	774	683	623	563	482	82	94	154	214
Range	0.088	0.069	0.058	23	26	26	26	12	15	2	2	2

Table 7: Selected CMCs of Thirteen Weld Metals with Ti-B-Al-N-O Additions

Table 7 shows that all 13 WMs showed a regular progression of calculated transformation temperatures, wherein $A_{r3} > B_S > B_F > M_S$. The calculated Ouchi's A_{r3} temperature showed a narrow range, between 751 °C and 774 °C. A progressive increase in calculated T_S temperature occurred from weld O2, U, Y2, Z2, Y, Z, X, X2, V1, V2, O and U2.

Both welds Y and Z showed the calculated (Ouchi's) A_{r3} temperature at 760 °C, midway in the 751°C – 774 °C range. The O2 WM with 399 ppm (0.0399 wt-%) O and 235 ppm (0.0235 wt-%) N showed the lowest calculated A_{r3} temperature at 751 °C but was closer to the experimentally determined T_S temperature at 754 °C.

Weld ID		Weld Metal Tensile Properties				CVN Test Temperature (°C)	
	YS (MPa)	UTS (MPa)	YS/UTS	El (%)	RA (%)	T_{100J} /°C	T_{28J} /°C
O	445	528	0.84	28	78	-14	-42
O2	505	607	0.83	24	76	20	-16
X	504	577	0.87	26	80	-61	-77
X2	578	631	0.92	25	78	-30	-58
Y	546	594	0.92	25.8	73.0	-84	-114
Y2	539	605	0.89	23.9	71.6	-24	-56
Z	610	640	0.95	27.2	73.4	-83	-100
Z2	493	583	0.85	26.8	69.2	13	-18
U	517	586	0.88	23	78	-53	-80
U2	474	541	0.88	28	73	-52	-81
V	668	732	0.91	20.3	69.7	-12	-46
V1	571	644	0.89	25	74	-64	-93
V2	529	591	0.90	25.6	73.8	-45	-70
Low	445	528	0.83	20.3	69.2	-83	-114
High	668	732	0.95	28	80	20	-16
Range	223	204	0.12	7.7	10.8	103	84

Table 8: Tensile and CVN Impact Properties of Thirteen Weld Metals with Ti-B-Al-N-O Additions

Table 8 shows the tensile and CVN impact properties of the 13 WMs. Weld O showed the lowest UTS at 528 MPa, consistent with its low alloy content. Weld V showed the highest UTS at 732 MPa. Correspondingly, a progressive decrease in UTS from 732 MPa to 528 MPa occurred among these welds. In particular, the CVN impact properties show T_{100J}/°C and T_{28J}/°C that achieved -84 J and -114 J absorbed energy. The 13 WMs showed T_{100J}/°C absorbed energy varied from -83 °C to +20 °C, while T_{28J}/°C absorbed energy varied from -114 °C to -16 °C. A review of the CVN impact test results revealed that welds Y and Z likely had "nearly" balanced Ti, B, Al, N and O additions that further reduced the TS temperature to 710 °C, as shown in Table 6.

Considering that welds Z and Y showed minimal N content at 67 ppm (0.0067 wt-%) and 83 ppm (0.0083 wt-%) respectively, and excellent CVN impact toughness, one could consider welds Z and Y as offering the most desirable baselines for the selection of WM compositions with "nearly" balanced Ti-B-Al-N-O additions.

Weld ID	Ti Content (wt-%)	B Content (wt-%)	Al Content (wt-%)	N Content (wt-%)	O Content (wt-%)	(Ti+B+Al+N+O) (wt-%)	UTS (MPa)	CVN Test Temperature		Transformation Temperature (°C)		
								T_{100J}/°C	T_{28J}/°C	T_S	T_F	(T_S- T_F)
O	0.0001	0.0001	0.0006	0.0079	0.0475	0.0562	528	-14	-42	762	554	208
O2	0.0005	0.0005	0.0005	0.0235	0.0399	0.0649	607	20	-16	754	534	220
X	0.041	0.0002	0.0001	0.0077	0.0282	0.0772	577	-61	-77	760	568	192
X2	0.045	0.0002	0.0005	0.0249	0.0297	0.1003	631	-30	-58	760	572	188
Y	0.039	0.0039	0.0013	0.0083	0.0308	0.0833	594	-82	-114	710	560	150
Y2	0.041	0.0044	0.0005	0.0232	0.0292	0.0983	605	-24	-56	703	510	193
Z	0.042	0.0048	0.016	0.0067	0.0438	0.1133	640	-83	-100	710	550	160
Z2	0.047	0.0045	0.018	0.023	0.044	0.1365	583	13	-18	703	560	143
U	0.039	0.0158	0.0005	0.0084	0.029	0.0927	586	-53	-80	700	531	169
U2	0.039	0.0167	0.0005	0.0217	0.0297	0.1076	541	-52	-81	765	574	191
V	0.054	0.0056	0.058	0.0041	0.044	0.1657	732	-12	-46	680	507	173
V1*	0.048	0.0044	0.056	0.012	0.0473	0.1677	644	-64	-93	760	555	205
V2	0.043	0.0035	0.056	0.0235	0.047	0.173	591	-45	-70	754	588	166
Low	0.0001	0.0001	0.0001	0.0041	0.0282	0.0562	528	-83	-114	680	507	143
High	0.054	0.0167	0.058	0.0249	0.0475	0.173	732	20	-16	765	588	220
Range	0.0539	0.0166	0.0579	0.0208	0.0193	0.1168	204	103	84	85	81	77

* The transformation temperature for weld V1 obtained from graphical interpolation of the curve shown in Ref. 60.

Table 9: Test Results of Thirteen WMs at 13°C/s Cooling Rate

Table 9 also shows WM UTS predicted using experimentally determined T_S temperatures using Eq. 6 with excellent correlation. These results illustrate the utility of Eq. 6 and Eq. 13 in designing the chemical composition of welding electrodes and WMs to achieve higher performance. While considering Ti-B-Al-N-O additions it may be wiser to avoid both rich and lean ends for all these micro-alloy elements. Particularly, excessive Al additions over 500 ppm (0.05 wt-%) as in welds V, V1 and V2 could potentially result in free Al in solution that could seriously harm CVN impact (or fracture) toughness. Furthermore, considering the need for effective deoxidation and de- nitrogenation, particularly when both O and N contents remain high as in welds V1 and V2, it may be necessary to ensure adequate additions of Ti and Al to tie-up O, besides additions of B and Al to tie-up N. Here, Ti addition is known to protect B from oxidation while allowing B to react with N thus reducing free nitrogen in solution.

Furthermore, soluble B is known to preferentially segregate to prior austenite grain boundaries and retard the nucleation of grain boundary ferrite during austenite to acicular ferrite transformation. A comparative dilatometric evaluation of transformation kinetics of welds V, V1 and V2 showed that balancing N content versus B and Ti contents retarded the experimentally determined T_S temperature associated with the formation of grain boundary ferrite in welds V1 and V2, further enabling the formation of a refined WM microstructure with predominantly AF and improved CVN impact toughness compared to weld V.

8.3 Dilatometric Evaluation of Thirteen WMs with Ti-B-Al-N-O Additions

The dilatometric evaluation showed fraction austenite that transformed to acicular ferrite versus transformation temperature for the 13 (O, O2, X, X2, Y, Y2, Z, Z2, U, U2, V, V1 and V2) WMs. As shown in Figure 8, between 0.2 and 0.8 fraction ferrite, the dilatometric curves for welds V2, Z and Z2 showed somewhat a steeper gradient. This steeper gradient is associated with a

"cloudburst" of austenite-to-ferrite phase transformation over a narrow (T_S-T_F) temperature range, with intragranular nucleation and growth of acicular ferrite, aided by balanced Ti-B-Al-N-O additions.

Nitrogen addition at more than 100 ppm (0.01 wt-%) is seen deleterious to WM CVN impact toughness However, it could be turned beneficial when B at about 40 ppm (0.004 wt-%) and Ti at about 400 ppm (0.04 wt-%) were added. Weld Z2 showed the lowest difference between T_S and T_F temperatures at 143 °C. Weld Y showed a 150 °C difference while weld Z showed a 160 °C difference for ($T_S - T_F$), and a lower N content. Here, the Ti-B-Al-N-O additions appeared to provide "a balance" that was perhaps quite effective in producing a "cloudburst" that likely aided the formation of acicular ferrite microstructure over a narrow ($T_S - T_F$) temperature range.

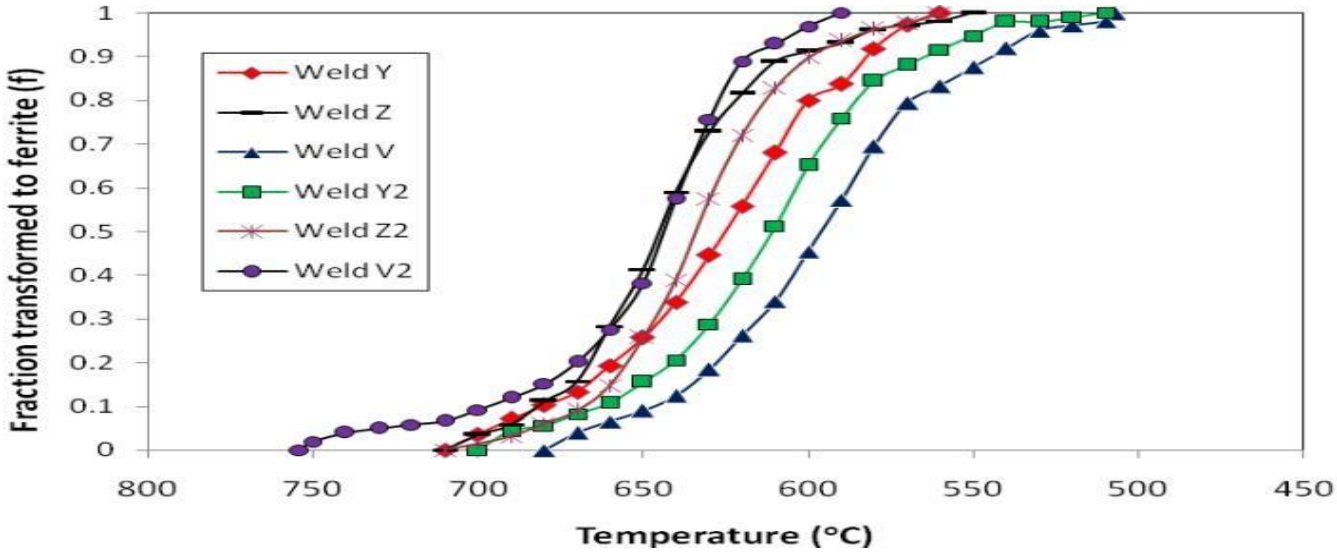

Figure 8: Dilatometric Evaluation of Austenite-to-Acicular Ferrite Transformation

Figure 9 showed that when the N content of WM was below 85 ppm (0.0085 wt-%), the overall trend between T_S temperature and UTS among all 7 welds was highly correlated Two of these 7 WMs (including weld W) with limited N content below 85 ppm (0.0085 wt-%), in particular, welds Z (with 640 MPa UTS) and Y (with 594 MPa UTS) appeared closer and on either side of the trend line indicating that their Ti, B, Al, O and N additions are well balanced, or adequately balanced in these 2 WMs. The trendline equation showed:

Weld metal UTS (in MPa) = 1768.7 – (1.6331 x T_S in °C), with r^2 = 0.683 (Eq. 13)

thereby clearly confirming the metallurgical principle that lowering the transformation temperature aided to increase WM UTS. The trendline also indicated that a T_S temperature lower than 680 °C achieved a WM UTS higher than 700 MPa (100 ksi).

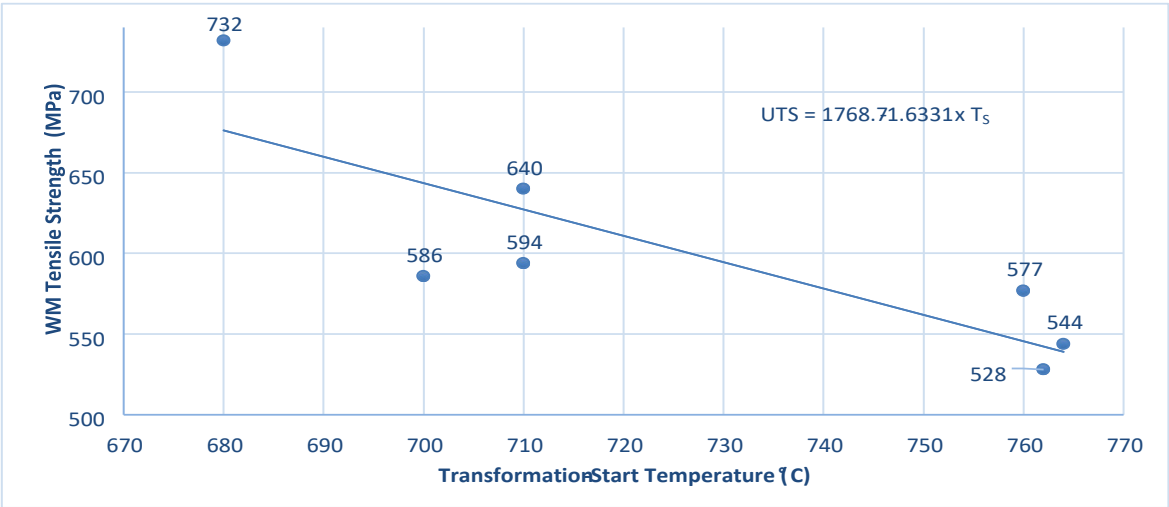

Figure 9: Effect of Transformation-Start Temperature on Weld Metal Tensile Strength (In Mpa)

As seen in Table 9, the balancing of Ti, B, Al, and O additions maybe related to T_S, with a decreasing T_S requiring a lower amount of Ti, B, Al, and O additions. As revealed by weld V, when T_S is at its low end, excessive amounts of Ti, B, Al, and O additions likely raised T_{28J}/°C indicating the possibility to form numerous inclusions that likely produced a "dirty weld." By contrast, as revealed by weld O, when T_S is at its high end, inadequate amount of Ti, B, Al, and O additions likely raised T_{28J}/°C indicating the possibility of free oxygen in solution.

Weld ID	Transformation-Start (A_{r3}) Temperature (°C)		Experimental WM UTS (MPa)	Predicted WM UTS (MPa)	
	Dilatometry (T_S)	Calculated *New* A_{r3}*		Based on (T_S) temperature from dilatometry**	Based on Calculated *New* A_{r3} temperature**
O	762	750	528	550	560
O2	754	739	607	557	570
X	760	736	577	551	573
X2	760	745	631	551	565
Y	710	724	594	597	584
Y2	703	731	605	603	578
Z	710	727	640	597	582
Z2	703	739	583	603	571
U	700	703	586	606	603
U2	765	720	541	547	588
V	680	728	732	624	580
V1	760	735	644	551	574
V2	754	754	591	557	557
Low	680	703	528	547	557
High	765	754	732	624	603
Range	85	51	204	77	46

* Calculated New Ar3 Temperature is based on Eq. 6.
**Predicted WM UTS value is based on Eq. 13.

Table 10: Experimental and Predicted T_S Temperatures and UTS of 13 Weld Metals with Ti-B-Al-N-O Additions

Table 10 shows the numerical values of transformation temperatures obtained from dilatometry and predicted using Eq. 6 with excellent correlation. Incidentally, as shown in Table 10 for U2 weld, a comparison of the experimentally determined T_S temperature at 765 °C and the calculated *New* A_{r3} temperature at 720 °C indicated a relatively wider difference in T_S temperature, meaning N addition seemed to nullify the beneficial effects of Ti, B, Al, and O additions in substantially lowering the T_S temperature, as opposed to the calculated *New* A_{r3} temperature of welds U, Y and Z. Although weld V showed the largest difference between experimentally determined T_S temperature and calculated *New* A_{r3} temperature and a low N content at 41 ppm (0.0041 wt-%), an excessive Ti content at 540 ppm (0.054 wt-%) likely resulted in higher T_{100J}/°C and T_{28J}/°C.

A recent research effort at Aachen University obtained tensile test results of weldments produced using GMAW process at two levels of energy input and the following set of 5 welding electrodes: G3Si, G Mn3Ni1Mo, G Mn4Ni1.5CrMo, G Mn4Ni2CrMo and G Mn4Ni2.5CrMo belonging to DIN EN ISO 16384:2012 specification (*Welding consumables—Wire electrodes, wires, rods and deposits for gas shielded arc welding of high strength steels—Classification*) and M21 ArC18 (i.e., Ar-18 % CO2) shielding gas per DIN EN ISO 14175 (Welding consumables — Gases and gas mixtures for fusion welding and allied processes) [64,65].

This effort experimentally determined the transformation-start T_S (i.e., A_{r3}) temperatures of the 5 sets of WM. Figure 10 shows a plot of tensile strength versus experimentally determined T_S temperature. As expected, the plot offered additional support for the inverse linear relationship between A_{r3} temperature and the resulting WM tensile strength. WM compositions were reported for 4 of these 5 welds but not for all 16 elemental compositions in the Evans's database. Their calculated (B_F - M_S) temperatures based on the reported listing of WM chemical compositions ranged between 36 °C and -23 °C.

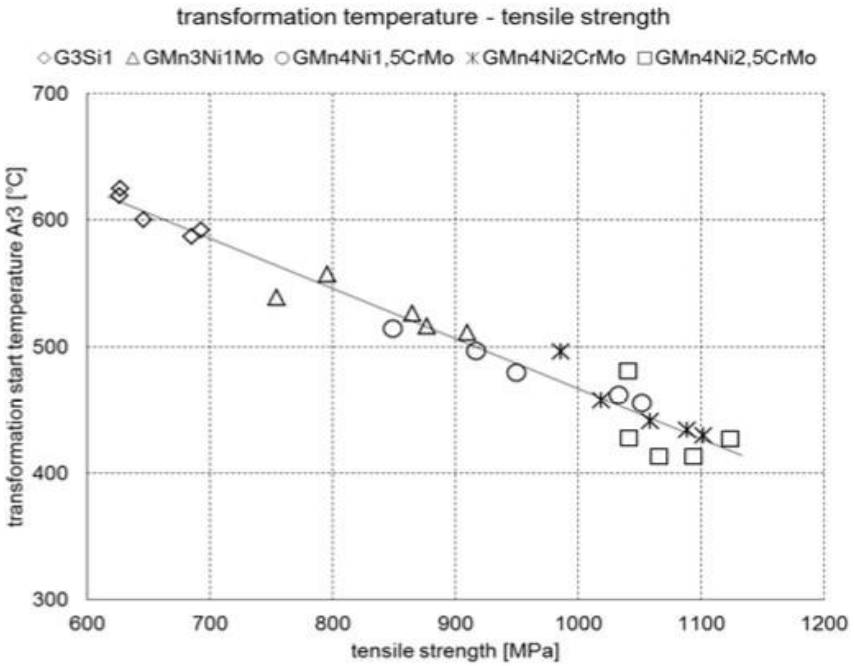

Figure 10: Inverse Linear Relationship between Experimentally determined A_{r3} Temperature and WM Tensile strength.

9. CVN Impact Temperature Prediction

Attempts to directly correlate transformation temperature with T_{100J} /°C and T_{28J} /°C for CVN absorbed energy of various WMs in Evans's SMA WM database didn't readily offer a clear trend. Lower shelf energy is generally controlled by microstructural features, while upper shelf energy is controlled mostly by the presence of inclusions and second phase particles that form cup and cone features during fracture, showing ductile dimples. Here, one could use the JWES-ANN template to identify and/or ascertain the "balanced" Ti-B-Al-N-O additions that predict a lower T_{28J} /°C CVN absorbed energy colder than -80 °C while ensuring that the error values associated with predictions were much less than 30 °C for each of these welds. In other words, one could achieve below -80 °C as a benchmark for T_{28J} /°C CVN absorbed energy to distinguish welds with balanced Ti, B, Al, N, and O contents.

Weld ID	T_S Temperature (°C) determined by Dilatometry	Experimental CVN Test Temperature (T_{28J}/°C)	CVN Test Temperature (T_{28J} / °C)		
			JWES Predicted Value for Original Weld	JWES Predicted Value as in Balanced Weld Y	JWES Predicted Value as in Balanced Weld Z
O	762	-42	-49	-88	-82
O2	754	-16	-15	-99	-88
X	760	-77	-80	-96	-90
X2	760	-58	-59	-95	-89
Y	710	-114	-102	--	-94
Y2	703	-56	-54	-95	-89
Z	710	-100	-94	-103	-
Z2	703	-18	-28	-95	-89
U	700	-80	-79	-99	-92
U2	765	-81	-78	-89	-84
V	680	-46	-47	-103	-95
V1	760	-93	-93	-96	-90
V2	754	-70	-71	-96	-90

Table 11: Predicted CVN Test Temperature of 13 TiBAlN Series WMs with Balanced Ti-B-Al-N-O Additions

For example, Table 11 shows a comparison of the actual test values and predicted results of T_{28J} /°C for all the 13 original welds with Ti-B-Al-N-O additions, corresponding to weld Y [with a total (Ti+B+Al+N+O) content at 0.0833 wt-%] and weld Z [with a total (Ti+B+Al+N+O) content at 0.1133 wt]. The predicted values for the 13 original welds based on JWES ANN were quite consistent with actual test results in both values and trend, and the error values associated with predictions were much less than 30 °C for each of these welds. Furthermore, when the Ti, B, Al, N, and O contents of all 12 WMs were modified to the same values as in weld Y [with a total (Ti+B+Al+N+O) content at 0.0833 wt-%] or weld Z [with a total (Ti+B+Al+N+O) content at 0.1133 wt], the predicted T_{28J}/°C for CVN absorbed energy for the welds decreased to temperatures below -80 °C in all WMs.

An alternate example involving a MnNi weld metal in Evans's SMA WM database showed 0.052 wt-% C, 0.3 wt-% Si, 1.44 wt-% Mn, 0.03 wt-% Cu, 3.46 wt-% Ni, 0.03 wt-% Cr, 0.005 wt-% Mo, 0.002 wt-% (20 ppm) Nb, 0.012 wt-% (120 ppm) V, 0.0055 wt-% (55 ppm) Ti, 0.0002 (2 ppm) wt-% B, 0.0005 wt-% Al, N at 0.008 wt-% (80 ppm), and O at 0.039 wt-% (390 ppm) with the following CMCs: CEN = 0.285; calculated B_{50} = 496 °C, calculated MS = 429 °C and a WM UTS at 682 MPa and T_{28J}/°C during CVN testing at -92 °C.

The JWES-ANN template for this WM showed T_{28J} /°C at an average of -87.2 °C. As shown in Fig. 11, when the principal elements of the WM chemical composition were marginally modified, thereby marginally increasing the calculated difference in (B_F - M_S) temperatures from 6 to 8 °C, the JWES-ANN template for the modified MnNi WM showed a further lowering of T_{28J} /°C to -96 °C. Actual measurement of BF and MS temperatures of the WM could offer additional support or metallurgical insight.

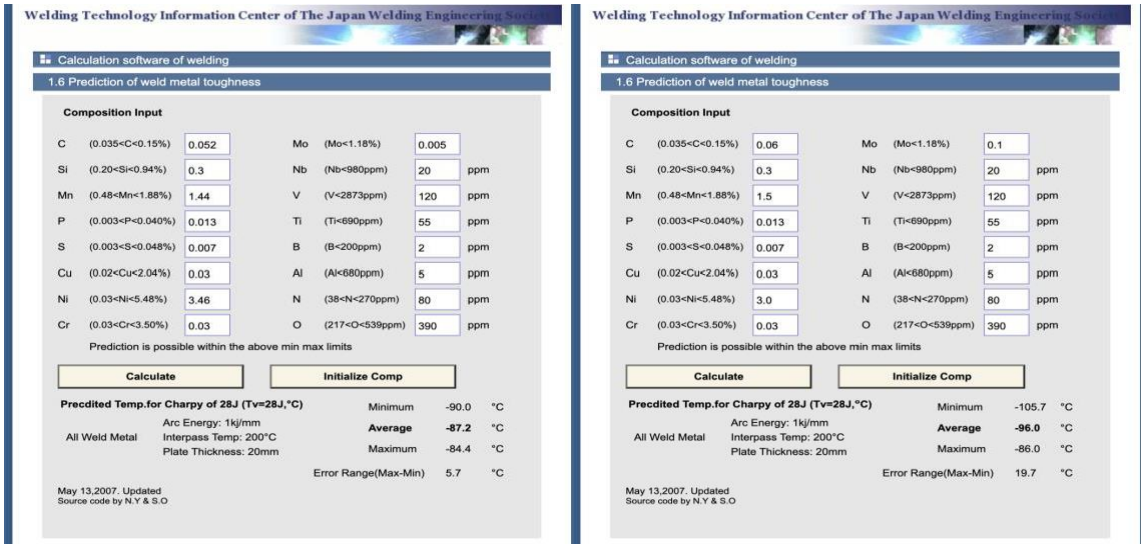

Figure 11: The JWES ANN predicted T_{28J}/°C. Left: Weld MnNi; Right: Modified Weld MnNi.

10. Two Tools to Ascertain Acicular Ferrite in Weld Metal

A recent research publication on "Influence of Microalloying on Precipitation Behavior and Notch Impact Toughness of Welded High-Strength Structural Steels," mentions the importance of AF in WM. This research article also emphasizes mechanical properties, especially CVN impact toughness of S690QL grade (per EN 10025-6) HSLA structural steel base metal (BM), WM and HAZ, that were evaluated to understand the influence of either Nb or Ti microalloying additions on the microstructure of the HAZ and its mechanical properties. A subsequent research publication on "Effect of Ti microalloying on the local strain behavior of cross-weld tensile samples determined by digital image correlation," further reinforced prior results of G69 solid wire electrode [66,67].

Element	C	Si	Mn	Cr	Cu	Mo	Ni	Al	Nb	Ti	N	CET[b]	CEV[b]
BM: Stand.[a]	0.20	0.80	1.70	1.50	0.50	0.70	4.0		0.06	0.05	0.015		0.65
BM: Ref	0.09	0.30	1.61	0.18	0.02	0.30	0.19	0.10	-	-	0.0063	0.30	0.47
BM: A (Nb)	0.07	0.29	1.54	0.17	0.02	0.29	0.18	0.10	0.025	-	0.0059	0.27	0.43
BM: B (Ti)	0.07	0.30	1.53	0.17	0.02	0.30	0.19	0.10	-	0.015	0.0055	0.27	0.44
WM: G69[c]	0.09	0.43	1.32	0.2	0.09	0.55	1.43	0.002	0.001	0.019	0.007	0.33	0.56

[a]EN 10025–6 S690QL

[b]EN 1011–2

[c]EN ISO 16834-A-G 69 6 M Mn4Ni1.5CrMo, chemical composition in accordance with the manufacturer's test report

Table 12: Chemical Composition (in wt-%) of Tested Materials (Fe balance) Determined Using Optical Emission Spectroscopy

As shown in Table 12, the WM chemical composition from welding electrode (G69) was low in Mn content (at 1.32 wt-%) but somewhat high in Ni content (1.43 wt-%) and had C content at 0.09 wt-%. However, these results were based on manufacturer's test report, and one is not certain what type of base metal was used in the manufacturer's test report, and whether the base metal dilution caused Nb and/or Ti micro-alloy additions in WMs. Readers might wonder why the authors didn't report the actual chemical composition vis-a-vis actual mechanical properties of the WMs as they related to each of three different variations of BMs. Furthermore, the reason why the authors didn't report 3 specific types of BM with additional Nb or Ti addition, with related dilution effect and corresponding WM chemical compositions is unclear.

Property	Yield strength, $R_{p0.2}$ (MPa)	Tensile strength, *Rm* (MPa)	Elongation at fracture, *A*5 (%)	Impact toughness, *Av*: − 40 °C (J)	Hardness (HV)
BMs[a]	690	770 to 940	14	Min. 27	284.2 (HV1)[c]
WM: G 69[b]	733	811	21.4	87.7 (64 J at − 60 °C)	264.3 (HV10)

[a]EN 10025–6 S690QL, properties in accordance with the standard

[b]EN ISO 16834-A-G 69 6 M Mn4Ni1.5CrMo, properties from the producer's test report

[c]Hardness testing

Table 13: Mechanical Properties of the Tested Materials

Table 13 listed the mechanical properties of BM and WM based on producer's test report.

The YS/UTS ratio of the WM was marginally higher than 0.90. The WM CVN impact toughness is reported at 87.7 Joules at -40 °C or 64 Joules at -60 °C. Figure 12 in shows the CVN impact toughness. The authors attribute the "relatively high impact energies of all investigated WM samples" to "the predominant AF microstructure, which is characterized by its high toughness compared to bainite." The WM fracture surfaces show variations in fibrous (F) zone, (S) shear lip zone, and (R) radial zone, each reported in % indicating Ti addition from base metal dilution in WM is marginally beneficial compared to Nb addition from base metal dilution.

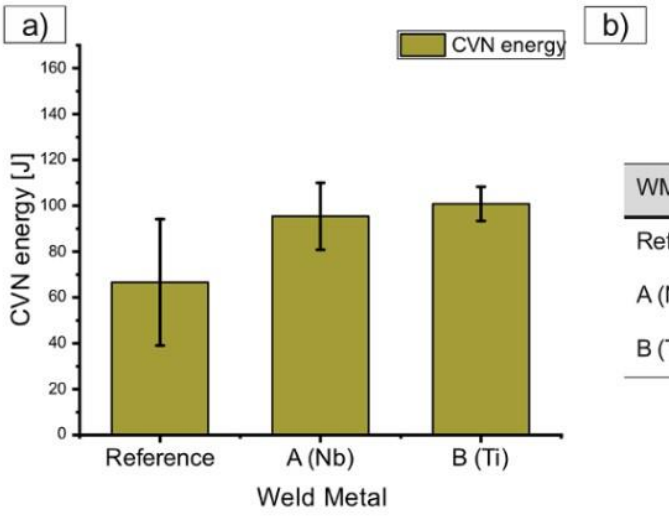

WM	F [%]	S [%]	R [%]
Reference	24	35	41
A (Nb)	26	39	35
B (Ti)	20	40	40

Figure 12: a) Impact Energy of three Investigated WMs and b) Fracture Surface Fractions of three Investigated WMs

One could apply the JWES-ANN template for this WM composition as well, although the JWES-ANN template had been developed only for SMA welding of 20 mm thick plates, interpass temperature at 200 °C and arc energy at 1 kJ/mm with a weld CR at 13 °C/s. Furthermore, the listing for G69 WM composition included only 11 elements (C, Si, Mn, Cr, Cu, Mo, Ni, Al, Nb, Ti and N) and didn't include P, S, V, B and O contents. A simple manipulation of P and S contents at 0.007 wt-%, Cr content at 0.03 wt-%, B content at 19 ppm (0.0019 wt-%) with a Ti:B ratio at 10:1, with O content at 290 ppm (0.0290 wt-%) leads to a test temperature for 28 Joules CVN impact toughness at a temperature colder than -116 °C.

Figure 13 shows the application of JWES-ANN tool for a typical WM composition with a total (Ti+B+Al+N+O) content at 579 ppm (0.0579 wt-%), and further based on a set of citations made by Ito, et al. on O content Yamada, et al. on Ti and B contents and Takada, et al. on Al content [68-70]. However, the Al content in Figure 13 is only at 10 ppm (0.001 wt-%). Due to high Mn content at 1.32 wt-%, Ti content at 190 ppm (0.019 wt-%) and O at 290 ppm (0.029 wt-%), perhaps $MnTi_2O_4$-rich spinel structures aided the formation of AF. This WM composition with a Ti:B ratio at 10:1, showed a predicted T_{28J}/°C colder than -116 °C, subject to experimental verification [71-72].

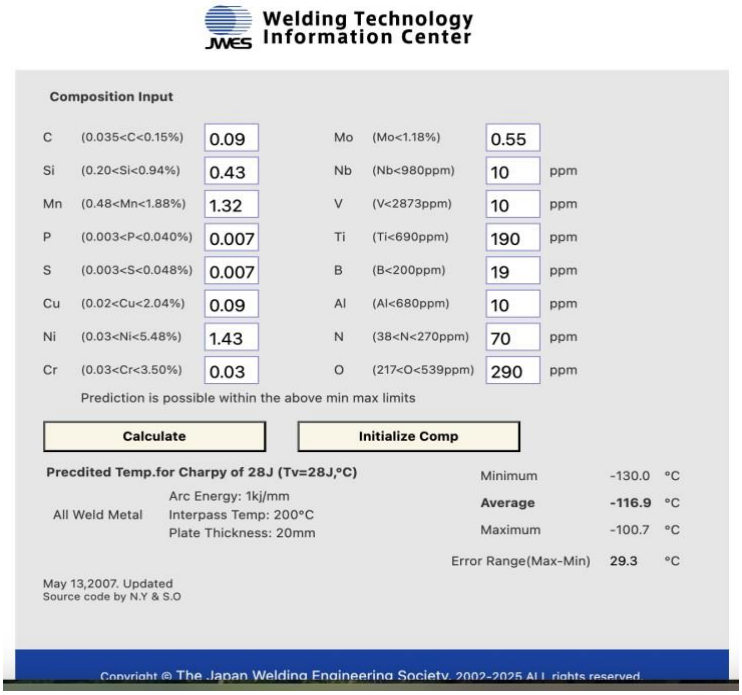

Figure 13: A Typical G69 Weld Metal Composition With A Predicted T_{28j}/°C Colder Than -116 °C

Furthermore, one could also apply the *New* A_{r3} regression equation that is dependent on the presence of the above 14 elements (excluding P and S). Gas metal arc (GMA) welding at 1 kJ/mm energy input and preheat and interpass temperature at 100 °C with 82% Ar-18% CO_2 as shield gas mix showed a $\Delta t_{8/5}$ time (measured by laser pyrometer) at 7.8 s which indicated a weld CR at 38.46 °C/s which is often higher than 13 °C/s for shielded metal arc WMs, as reported by N. Ilman et al.

Application of the *New* A_{r3} equation (Eq. 6) to the above WM composition as listed in the JWES-ANN template revealed a T_S temperature at 583 °C. Application of Eq. 13 on WM UTS (in MPa) = 1768.7 – (1.6331 x T_S in °C), with $r^2 = 0.683$ revealed a UTS of 816.60 MPa, which is marginally higher than 811 MPa UTS reported in.

Based on the above example, the Eq. 6 to calculate *New* A_{r3} temperature that embodies the effects of 14 major and minor alloy elements (in wt-%) besides weld CR (in °C/s) in achieving about 690 °C ± 40 °C temperature is expected to further complement the JWES-ANN template for predicting T_{28J}/°C for CVN absorbed energy based on WM chemical composition.

11. Summary

The two sets of Tables for compliance, one on Specified Electrode Chemical Composition Requirements and the other on Specified Minimum Weld Mechanical Properties Requirements in a welding electrode specification are not mutually exclusive. However, the underlying metallurgical principles keep them inter-dependent. These metallurgical principles are related to chemical composition primarily through austenite transformation-start T_S temperature, processing conditions during and following fusion welding, microstructure development and resultant mechanical properties such as WM tensile strength and CVN impact (or fracture) toughness.

The metallurgical design of welding electrodes for high strength steels further demonstrates that suppressing austenite transformation-start (T_S) temperatures simultaneously increases both strength and low-temperature impact toughness of HSS WM. Specifically, the metallurgical design recommends a two-step approach to achieve compliance with electrode specification requirements: the first step offers controlled lowering of various austenite T_S temperatures besides C content, and CEN for correlating specified electrode chemical composition requirements with specified minimum WM tensile property requirements. Using the set of constitutive equations involving the *New* A_{r3} equation and its relationship with WM UTS, one could control the amounts of principal alloy elements, so the relevant calculated austenite transformation-start (T_S) temperatures (e.g., A_{r3}, B_S and M_S) stay in a desirable range. While doing so, one also needs to ascertain that the common progression of calculated T_S temperatures where in $A_{r3} > B_S > M_S$ remains valid. Furthermore, dilatometric evaluations of selected WMs showed that balanced Ti, B, Al, N, O additions lowered the actual T_S temperature by about 60 °C compared to the calculated T_S (i.e., A_{r3}) temperature. At a N content below 85 ppm (0.0085 wt-%) both a lower T_S temperature and a narrow start-to-finish ($T_S - T_F$) temperature range achieved exceptional CVN impact toughness. Weld metal N content at more than 100 ppm (0.010 wt-%) effectively nullified the beneficial effects of Ti, B, and Al additions in lowering the T_S temperature.

The above two computational tools can be used with minimal risk in the efficient development and/or evaluation of welding electrode compositions based on Fe–C–Mn system that would likely provide essential microstructure in WM to meet or exceed the requirements for high-performance and demand-critical applications. The second step offers ANN template provided by JWES at its website to manipulate WM compositions and balance the Ti, B, Al, N, O additions in specified ranges, thereby ascertain further lowering of T_{28J}/°C in CVN testing below -80 °C.

In summary, while developing or identifying high-strength, high-performance welding electrodes for HSS, one should consider several complex interactive effects of various alloy elements during fusion welding conditions, their combined effects on WM microstructure development and weldability of HSS. To successfully meet or exceed specific HSS weld metal mechanical properties requirements as specified in a relevant welding electrode specification, one should:

- Avoid "rich" and "lean" compositions in relevant welding electrode specifications
- Control principal alloy elements to suppress the calculated or actual Ts temperature, ensuring the progression of calculated $A_{r3} > B_S > M_S$ remains valid
- Keep C content below 0.10 wt-% to enhance weldability
- Reduce N content below 100 ppm
- To achieve UTS less than 700 MPa, keep CEN below 0.300
- To achieve UTS greater than 700 MPa, keep CEN above 0.320
- To achieve UTS over 700 MPa, keep the calculated difference in (B_F - M_S) temperatures between -20 °C and -50 °C
- Use the JWES ANN template to balance Ti, B, Al, and O contents as determined by the predicted lowering of T_{28J}/°C to -60 °C during CVN testing.

The above metallurgical understanding to electrode and WM design is recommended to enable one to achieve a lower Ts and a lower (T_s-T_F) range when an exceptional combination of high strength and superior toughness can be simultaneously realized for a given C content and CEN.

The New regression equation to calculate *New* A_{r3} temperature that embodies the effects of both major and minor alloy elements (in wt-%) besides weld cooling rate (in °C/s) appears extremely useful in allowing a larger control over selection of chemical composition of welding electrodes and fusion welding processing conditions, and to relate the calculated *New* A_{r3} temperature with WM microstructure development and resultant WM UTS.

The advent and continued growth of various modern computational technologies such as Machine Learning and ANN are expected

to allow further development of new and more useful regression equations for controlled lowering of T_s temperature.

References

1. Sampath, K. (2025). Three Essential Steps in Metallurgical Design of Solid Wire Electrodes for High Strength Steels. *Aspects in Mining & Mineral Science, 14*(1), 1694-1699.
2. Schank, J. F., Ip, C., Lacroix, F. W., Murphy, R. E., Arena, M. V., Kamarck, K. N., & Lee, G. T. (2011). Learning from Experience, Volume 2: Lessons from the US Navy's" Ohio,"" Seawolf," and" Virginia" Submarine Programs.
3. AWS D1.8/D1.8M:2016, Structural welding code-seismic supplement, American Welding Society, Miami, FL
4. Ohaeri, E. G., & Szpunar, J. A. (2022). An overview on pipeline steel development for cold climate applications. *Journal of Pipeline Science and Engineering, 2*(1), 1-17.
5. Lalam, S. H. (2000). Modelling of mechanical properties of ferritic weld metals. *Ph. D. Thesis, University of Cambridge, October*.
6. Lalam, S. H., Bhadeshia, H. K. D. H., Evans, G. M., & MacKay, D. J. C. (2000). Estimation of mechanical properties of C-Mn weld metals, IIW Doc. II-A-072-00.
7. Evans, G. M., & Bailey, N. (1997). *Metallurgy of basic weld metal*. Woodhead publishing.
8. Evans, G. M. (2015). *Database-Database—Weld metal composition and properties.*
9. Evans, G. M. (2018). A reassessment of the predictive Charpy-V toughness of the manganese-nickel weld metal combination. IIW Doc II-C-546–18.
10. Bhadeshia, H. K. D. H. (2007). Frontiers in the modelling of steel deposits. Journal of the Japan Welding Society, 76(2), 24-30.
11. Pickering, F. B. (1978). Physical metallurgy and the design of steels. (*No Title*).
12. Bramfitt, B. L. (1998). Structure/property relationships in irons and steels.
13. Yurioka, N., & Suzuki, H. (1983). Determination of necessary preheating temperature in steel welding.
14. OUCHI, C., SAMPEI, T., & KOZASU, I. (1982). The effect of hot rolling condition and chemical composition on the onset temperature of γ-α transformation after hot rolling. *Transactions of the Iron and Steel Institute of Japan, 22*(3), 214-222
15. Steven, W. (1956). The temperature of martensite and bainite in low-alloy steels. *Journal of the Iron and Steel Institute, 183*, 349-359.
16. Sugiyama, M., Sawa, G., Hata, K., & Maruyama, N. (2019, August). Heterogeneous microstructure of low-carbon lath martensite with continuous yielding behavior in Fe-C-Mn alloys. In *IOP Conference Series: Materials Science and Engineering* (Vol. 580, No. 1, p. 012045). IOP Publishing.
17. Jorge, J. C. F., De Souza, L. F. G., Mendes, M. C., Bott, I. S., Araújo, L. S., Dos Santos, V. R., ... & Evans, G. M. (2021). Microstructure characterization and its relationship with impact toughness of C–Mn and high strength low alloy steel weld metals–a review. *Journal of Materials research and technology, 10*, 471-501
18. Varadarajan, R., & Sampath, K. (2023). Application of machine learning to regression analysis of a large SMA weld metal database. Weld. J, 102, 31-52.
19. Bauné, E., Chovet, C., Leduey, B., Bonnet, C., & Germany, S. S. A. L. W. (2006). *Consumables for welding of (very) high strength steels mechanical properties of weldments in as-welded and stress-relieved applications, IIW Doc*. II-1696-06.
20. Ito, Y. (1968). Weldability formula for high strength steels related to heat affected zone cracking. *Doc. IIW IX-576-68.*
21. Dearden, J. (1940). A guide to the selection and welding of low alloy structural steels. *Institute of Welding Transactions, 3*, 203.
22. Sampath, K., & Varadarajan, R. (2023). High strength steel weld metal properties: metallurgical criteria and computational tools. *Welding in the World, 67*(9), 2081-2105.
23. Dai, T., Feng, Z., Kyle, D., David, S. A., Sebeck, K. M., Tzelepis, D. A., ... & Rogers, M. (2022). The toughness of high-strength steel weld metals. *Welding Journal, 101*(2).
24. Evans, G. M. (1980). Effect of manganese on the microstructure and properties of all-weld-metal deposits.
25. Evans, G. M. (1983). The Effect of Carbon on the Microstructure and Properties of C--Mn All-Weld Metal Deposits. *Weld. Res. Abroad, 19*(1), 13-24.
26. Evans, G. M. (1986). Effects of silicon on the microstructure and properties of C-Mn all-weld-metal deposits. *Metal Construction, 18*(7), 438R-444R.
27. Evans, G. M. (1988). Effect of molybdenum on microstructure and properties of C-Mn all-weld metal deposits. Joining and materials, 1, 239-46.
28. Evans, G. M. (1993). The effect of micro-alloying elements in C-Mn steel weld metal. WELDING IN THE WORLD-LONDON-, 31, 12-12.
29. Evans, G. M. (1995). Microstructure and properties of ferritic steel welds containing Al and Ti. *Welding Journal, 74*(8).
30. Evans, G. M. (1996). Microstructure and properties of ferritic steel welds containing Ti and B. *Welding journal, 75*(8).
31. Miettinen, J., Koskenniska, S., Somani, M., Louhenkilpi, S., Pohjonen, A., Larkiola, J., & Kömi, J. (2021). Optimization of the CCT curves for steels containing Al, Cu and B. *Metallurgical and Materials Transactions B, 52*(3), 1640-1663.
32. HJ, K. (2000). Effect of Mn and Ni on the variation of the microstructure and mechanical properties of low-carbon weld metals. *ISIJ international, 40*(12), 1237-1245.
33. Keehan, E., & Karlsson, L. (2005). New alloying concepts for high strength steel weld metals. *Super high strength steels.*
34. Keehan, E., Karlsson, L., Andrén, H. O., & Bhadeshia, H. K. D. H. (2005, May). Understanding mechanical properties of novel high strength steel weld metals through high-resolution microstructural investigations. In *International conference: trends in welding research.*
35. Keehan, E., Karlsson, L., & Andrén, H. O. (2006). Influence of carbon, manganese and nickel on microstructure and

properties of strong steel weld metals: part 1–effect of nickel content. *Science and Technology of Welding and Joining, 11*(1), 1-8.
36. Keehan, E., Karlsson, L., & Andrén, H. O. (2006). Influence of carbon, manganese and nickel on microstructure and properties of strong steel weld metals: part 1–effect of nickel content. *Science and Technology of Welding and Joining, 11*(1), 1-8.
37. Keehan, E., Karlsson, L., & Andrén, H. O. (2006). Influence of carbon, manganese and nickel on microstructure and properties of strong steel weld metals: part 1–effect of nickel content. *Science and Technology of Welding and Joining, 11*(1), 1-8.
38. Fujii, H., & Ichikawa, K. (2001). Estimation of weld properties by bayesian neural network. *Welding international, 15*(12), 935-939.
39. Lalam, S. H., Bhadeshia, H. K. D. H., & MacKay, D. J. C. (2000). Estimation of mechanical properties of ferritic steel welds. Part 1: Yield and tensile strength. *Science and technology of welding and joining, 5*(3), 135-147.
40. Lalam, S. H., Bhadeshia, H. K. D. H., & MacKay, D. J. C. (2000). Estimation of mechanical properties of ferritic steel welds. Part 2: Elongation and Charpy toughness. *Science and technology of welding and joining, 5*(3), 149-160.
41. Metzbower, E. A., DeLoach, J. J., Lalam, S. H., & Bhadeshia, H. K. D. H. (2001). Neural network analysis of strength and ductility of welding alloys for high strength low alloy shipbuilding steels. *Science and technology of welding and joining, 6*(2), 116-124.
42. Metzbower, E. A., DeLoach, J. J., Lalam, S. H., & Bhadeshia, H. K. D. H. (2001). Analysis of toughness of welding alloys for high strength low alloy shipbuilding steels. *Science and technology of welding and joining, 6*(6), 368-374.
43. Metzbower, E. A., DeLoach, J. J., Lalam, S. H., & Bhadeshia, H. K. D. H. (2002). Secondary Eeffects in Neural Network Analysis of the Mechanical Properties of Welding Alloys for HSLA Shipbuilding Steels. *BOOK-INSTITUTE OF MATERIALS, 784,* 231-242.
44. Kim, J. H., Jung, C. J., Park, Y. I., & Shin, Y. T. (2022). Development of closed-form equations for estimating mechanical properties of weld metals according to chemical composition. *Metals, 12*(3), 528.
45. Xiong, J., Zhang, T., & Shi, S. (2020). Machine learning of mechanical properties of steels. *Science China Technological Sciences, 63*(7), 1247-1255.
46. Online calculator for the Charpy impact transition temperature that satisfies the 28 J.
47. Sampath, K., Green, R. S., Civis, D. A., Williams, B. E., & Konkol, P. J. (1995). Metallurgical model speeds development of GMA welding wire for HSLA steel. *Welding journal, 74*(12), 69-76.
48. Sampath, S. K., & Civis, D. (1995). Evaluation of new high performance electrodes for GMA welding of HSLA-100 steel. *High Performance Structural Steels*, 179-188.
49. Sampath, K., & Green, R. S. (1998). U.S. Patent No. 5,744,782. Washington, DC: U.S. Patent and Trademark Office.
50. Sampath, K. (2005). Constraints-based modeling enables successful development of a welding electrode specification for critical navy applications. *Welding Journal, 84*(8), 131s-138s.
51. MIL-S-16216, Military Specification, Steel plate, alloy, structural, high yield strength (HY- 80 and HY-100)
52. NAVSEA Technical Publication T9074-BD-GIB-010/0300, Base materials for critical applications: Requirements for low alloy steel plate, forgings, castings, shapes, bars, and heads of HY- 80/100/130 and HSLA-80/100
53. MIL-E-23765/2E, Military Specification: Electrodes and Rods – Welding , Bare, Solid, or Alloy Cored; and Fluxes, Low Alloy Steel (22 April 1994)
54. Sampath, K., & Varadan, R. (2006). Evaluation of chemical composition limits of GMA welding electrode specifications for HSLA-100 steel. *Balance, 100*, 88.
55. Sampath, V., Kehl, J., Vizza, C., Varadan, R., & Sampath, K. (2008). Metallurgical design of high-performance GMAW electrodes for joining HSLA-65 steel. *Journal of materials engineering and performance, 17*(6), 808-819.
56. Sampath, K. (2021). Analysis of a high-strength steel SMAW database. *Welding Journal, 100*(12), 410-420.
57. Sampath, K. (2022). Metallurgical design rules for high-strength steel weld metals. *Weld. J, 101,* 123-143.
58. Ilman, M. N., Cochrane, R. C., & Evans, G. M. (2012). Effect of nitrogen and boron on the development of acicular ferrite in reheated C-Mn-Ti steel weld metals. *Welding in the World, 56*(11), 41-50.
59. Ilman, M. N., Cochrane, R. C., & Evans, G. M. (2014). Effect of titanium and nitrogen on the transformation characteristics of acicular ferrite in reheated C–Mn steel weld metals. *Welding in the World, 58*(1), 1-10.
60. Ilman, M. N., Cochrane, R. C., & Evans, G. M. (2015). The development of acicular ferrite in reheated Ti–B–Al–N-type steel weld metals containing various levels of aluminium and nitrogen. *Welding in the World, 59*(4), 565-575.
61. MQ, J., GM, E., & GR, E. (1995). The influence of titanium additions and interpass temperature on the microstructures and mechanical properties of high strength SMA weld metals. *ISIJ international, 35*(10), 1222-1231.
62. Oh, D. W., Olson, D. L., & Frost, R. H. (1990). The influence of boron and titanium on low-carbon steel weld metal. *Welding Journal, 69*(4), 151s-158s.
63. Sampath, K. (2024). Selective analysis of a high-strength steel shielded metal arc weld metal database. *Aspects in.*
64. Sharma, R., & Reisgen, U. (2017). Comparative study of phase transformation temperatures in high strength steel weld metals. *Materials Testing, 59*(4), 344-347.
65. Sharma, R., & Reisgen, U. (2017, February). Cooling curve based estimation of mechanical properties in high strength steel welds. In *Materials Science Forum* (Vol. 879, pp. 1760-1765). Trans Tech Publications Ltd.
66. Schroeder, N. Rhode, M. Kannengiesser, T. 2024. Influence of microalloying on precipitation behavior and notch impact

toughness of welded high-strength structural steels, Welding in the World, 68: pp. 2647-2659,
67. Schroeder, N., Rhode, M., Kannengiesser, T., Kromm, A., Kadoke, D., & Kruse, J. (2025). Effect of Ti microalloying on the local strain behavior of cross-weld tensile samples determined by digital image correlation. *Welding in the World,* 1-17.
68. Ito, Y., Nakanishi, M., & Komizo, Y. I. (1982). Effects of oxygen on low carbon steel weld metal.
69. Yamada, T., Terasaki, H., & Komizo, Y. I. (2009). Relation between inclusion surface and acicular ferrite in low carbon low alloy steel weld. *ISIJ international, 49*(7), 1059-1062.
70. Takada, A., Terasaki, H., & Komizo, Y. (2013). Effect of aluminium content on acicular ferrite formation in low carbon steel weld metals. *Science and Technology of Welding and Joining, 18*(2), 91-97.
71. Loder, D., Michelic, S. K., & Bernhard, C. (2017). Acicular ferrite formation and its influencing factors-a review. *Journal of Materials Science Research, 6*(1), 24-43.
72. Vezzù, S., Scappin, M., Boaretto, D., & Timelli, G. (2019). On the Effect of slight variations of Si, Mn, and Ti on inclusions properties, microstructure, and mechanical properties of YS460 C-Mn steel welds. *Metallography, Microstructure, and Analysis, 8*(3), 292-306.